We thank the reviewers and the editior for taking time to go through comment on the manuscript. Their comments and suggestions have greatly improved the quality of the manuscript

We have prepared a response to the reviewers comments and suggestions.

The reviewer comments/suggestions are in Italics and the responses have been provided in bold.

The authors have appropriately responded in their letter to most of my main concerns and have taken adequate steps in the paper to respond to them.

However, there are a few points that need further action so that the readers will be better able to get full benefit of this interesting study.

One important point is that what is compared in the 'observation-model' comparison is not obvious as written. I understood that it was the result of Craig-Gordon (or its extended version) with the 'global closure assumption' (at least, I thought that these were equations 7 and 18 which are used, and not 1 and 11). This should be specified, for example in the introduction on line 47 (and maybe in the captions for some of the corresponding figures).

- **The equations used are eq 7 for the Traditional Craig Gordon model and eq 18 for the Unified Craig Gordon Model. This has been mentioned in the introduction of the modified version and the caption of Fig 7 and Fig 8.**

I did not fully understand also what is done with Pfahl and Wernli's study. It is cited as if they were providing diffusivity coefficients. However, it is not what the 2009 paper is about. The values cited on line 136 are close to be the inverse of their non-equilibrium fractionation factors (a power-law m independent of wind speed, as discussed inPfahl and Wernli (2003) paper). The issue discussed in the paper is the dependence of the fractionation factor as a function of wind which is specific to each study (Merlivat and Jouzel (1979), Cappa et al (2003) and Pfahl and Wernli (2003). In this sense, discussing using Pfahl and Wernli is different from just a question of diffusivity coefficients, for which I am only aware of the two studies (Merlivat, 1978; Cappa et al., 2003). It is in itself a parameterization. How is this taken into account here?

- **In Pfahl and Wernli 2009, A comparison of the simulated deuterium excess with the measurements , the numerical values of the diffusivity ratios were calculated that lead to the best agreement between the observed and the simulated values. The best agreement was based on the r2 value for observed vs simulated d-excess in their study which they suggested to be used to calculate the isotopic composition of evaporation. The Merlivat, 1978; Cappa et al., 2003 diffusivity values were based on experimental studies while in the Pfahl and Wernli 2009 these values were calculated based on the r2 value of the simulated vs observed d-excess.**

what is variable 'x' is not really defined (cf lines 123 and 136: the definition of 'x'). As there is no equation for x, it is hard to estimate quantitatively what is the index x. A definition equation should be introduced once, also better defining the index and how it is used.

- **x is the turbulence index of atmosphere which signifies the proportion of vapor that escapes by isotopic fractionating molecular diffusion and non-fractionating**

turbulent diffusion. When x = 1 the vapor escapes solely by molecular diffusion and for x = 0 the vapor escapes only due to turbulent diffusion.

- **This has been added to the modified version**

The conclusion is rather short, and should be slightly expanded. I still think that one can mention there possible caveats (or modifications) to TCG or UCG models used for the evaporative flux. For example, sea spray formation and evaporation by very high winds are not taken into consideration. Same for condensation/deposition close to sea-ice at near-freezing temperatures (but probably only encountered at the most southern latitudes during these cruises). The advective mixing model is a very nice addition, nonetheless there can be other sources of advective humidity to the surface layers than from Antarctica (such as from upper atmospheric layers with different properties, in particular because of condensation/precipitation...) or reevaporation of rainfall. I am not saying by that these are necessarily important to take into consideration (after all, there still exists an average misfit wit hteh evaporation model both ind18O and d-excess on Figure 9, even north of 60°S). Also, the non-local source of the evaporation was discussed (with the back trajectories). This could be commented upon in the conclusion section (difference between local and 'non-local' sources.

- **The conclusion is expanded in the revised version.**

Also, there were some statistical relations which hold better when separating the two cruises. Any idea why?

- **This is probably due to the difference in the number of points used to calculate the regression parameters and the increased scatter when the both the cruises are considered together. Nonetheless the differences are not too large.**

Detailed comments:
In the reply letter, it is mentioned that some samples are from bucket collection, other from CTD cast. For buckets, could there be possible biases (in S and d18O, both too high), but also the two samples (S and d18O) are not collected with the same bucket. This should mentioned in the S table caption (adding for example a * to the salinities not collected from same bucket as the sample for d18O analysis). Otherwise, there are some anomalies in d18O/S that cannot be understood. For example; the low value d18O near an iceberg is not associated with low- S , which I would have assumed for this season, and if there no refreezing along the iceberg at depth (in this case, is it the S-value from a CTD cast or from a bucket; and is there or not refreezing, which would be interesting per se).

- **The salinity values included in the modified version are for the samples only from the bucket thermometer . We have not included the CTD salinity values. The bucket sampling was done every 6 hours during the expeditions along the transect which sometimes didn't coincide with the water vapor sampling, therefore a different bucket sample was used to collect the sample for 18O measurement for which we didn't measure the salinity. These samples have been marked in the revised version.**

At the end of the introduction, line 47, '... and different fractions of molecular vs turbulent diffusion.' I think that it is important to add 'in the framework of the global closure

assumption' (at least, I understood that these were equations 7 and 18 which are used, and not 1 and 11; this needs to be specified)

- **As mentioned earlier, the equations used are eq.7 and eq 18. This has been specified and suggestion included in the modified version.**

Line 96, suggestion to replace starting at 'ABove the ocean one can assume...' by 'The global closer assumption is commonly done, by which ...'

- **This sentence has been rephrased according to the suggestion.**

Line 136: I would change citation to Pfahl and Wernli.

- **Done**

Fig. 1: add year and dates in caption of fig. 1

- **The caption has been modified.**

Fig. 4: the end of the caption is unclear, as well as the response in the response letter. There may be a need to specify more how the data are grouped based on the trajectories (is the source latitude three days before considered, for example?)

- **The plot (d) has been removed from the modified Fig 4.**

FIgure 10: interesting, but I find what is written along the horizontal axis hard to read. Also, always the same sign (except for slope middle pattern). Nothing cut? Any idea why?

- **The text of the horizontal axis has been enlarged and it is clear now.**
- **This plot depicts the differences between the observed and modelled lope and intercept of the meteorological parameters and d-excess. While the difference between the modelled and the observed slopes is the less, the models is all the relationships underpredict the intercept values. This due to the combination of molecular diffusivity and turbulence index values used in the Craig-Gordon equations.**

Figure 11: why the choice of a blue column, and not just blue dots? This would be more consistent with earlier figures and also easier to visualize.

- **The figure has been modified according to the suggestion.**

l. 151: remove 'were'

- **Done**

l. 152: replace 'like' by 'such as'

- **Done**

l. 167: remove 'caused'

- **Done**

l. 170, and L. 187: SST instead of sst

- **Done**

l. 197: 'that' instead of 'than'

- **Done**

l. 215: 'd-excess of' to be replaced by 'and d-excess'

- **Done**

l. 217: 'observations' and later 'links'

- **Done**

l. 225: 'that predict'

- **Done**

l. 229: end of sentence 'are considered'?
- **Done**

l. 234: '... is insufficient...'
- **Done**

l. 235: remove 'The process like' and start sentence by 'Advective mixcing...'
- **Done**

l. 253: replace 'the contribution of which' by 'its contribution....' or something equivalent
- **Rephrased**

Suppl. Material:
for humidity, sling psychrometer used. What is the accuracy expected for its reading?
SST from bucket thermometer. The authors mention that it is accurate to 0.2°C? How is the bucket collected and its temperature read when there is high wind (more risk of cooling... evaporation?) I dont think that it will be as acurate with winds of 25 m/s or more that were sometimes encountered.
- **There was a mistake in the accuracy of the psychrometer and the bucket thermometer. The values were interchaged. The accuracy of the bucket thermometer is 0.5^0 while for the sling psychrometer 0.2^0C. This has been corrected in the modified supplementary file.**
- **Empirical Relation used to calculate the Relative Humidity with expected accuracy of 2- 3% with accuracy 0.2° C of the sling Psyhcrometer.**
- **The bucket thermometer is lowered with the rope attached to it until it is immersed in the water for 5-10 minutes to get well mixed water. The bulb of the thermometer is at the bottom of the bucket and hence evaporative cooling due to high wind speed will happen at the surface and will not influence the measurements.**

In table 4, the dates starting in the middle of the table invert month and day. There is also an incorrect date one line before the end.
- **These have been corrected in the modified version.**

Craig-Gordon model validation using stable isotope ratios in water vapor over the Southern Ocean

Shaakir Shabir Dar[1], Prosenjit Ghosh[1,2], Ankit Swaraj[2], and Anil Kumar[3]

[1]Centre for Earth Sciences, Indian Institute of Science, Bengaluru, 560012, Karnataka, India.
[2]Divecha Centre for Climate Change, Indian Institute of Science, Bengaluru, 560012, Karnataka, India.
[3]National Centre for Polar and Ocean Research, Vaso-da-Gama, 403804, Goa, India.

Correspondence: Prosenjit Ghosh (pghosh@iisc.ac.in)

Abstract. The stable isotopic composition of water vapor over a water body is governed by the isotopic composition of surface water, ambient vapor isotopic composition, exchange and mixing processes at the water-air interface as well as the local meteorological conditions. These parameters form inputs to the Craig-Gordon models, used for predicting the isotopic composition of vapor produced from the surface water due to the evaporation process. In this study we present water vapor, surface water isotope ratios and meteorological parameters across latitudinal transects in the Southern Ocean (27.38°S to 69.34°S and 21.98°S to 66.8°) during two austral summers. The performance of Traditional Craig-Gordon (TCG) (Craig and Gordon, 1965) and the Unified Craig-Gordon (UCG) (Gonfiantini et al., 2018) models is evaluated to predict the isotopic composition of evaporated water vapor flux in the diverse oceanic settings. The models are run for the molecular diffusivity ratios suggested by (Merlivat, 1978) (MJ), (Cappa et al., 2003) (CD) and (Pfahl and Wernli, 2009) (PW) and different turbulent indices (x) i.e. fractional contribution of molecular vs turbulent diffusion. It is found that the $UCG^{MJ}_{x=0.8}, UCG^{CD}_{x=0.6}, TCG^{MJ}_{x=0.6}$ and $TCG^{CD}_{x=0.7}$ models predicted the isotopic composition that best matches with the observations. The relative contribution from locally generated and advected moisture is calculated at the water vapor sampling points, along the latitudinal transects, assigning the representative end member isotopic compositions and by solving the two-component mixing model. The results suggest varying contribution of advected westerly component with an increasing trend up to 65°S. Beyond 65°S, the proportion of Antarctic moisture was found to be prominent and increasing linearly towards the coast.

1 Introduction

The knowledge of factors governing the evaporation of water from the oceans is an essential part of our understanding of the hydrological cycle. The oceans regulate the climate of the earth through heat and moisture transport (Chahine, 1992). Nearly $\approx 97\%$ of the water of earth is in the oceans as saline while the residual $\approx 3\%$ is fresh water stored in groundwater, glaciers and lakes, or flowing as rivers and streams (Korzoun and Sokolov, 1978). Evaporation of ocean water generates vapour and forms the initial reservoir for circulation in the hydrological cycle. A fraction of this vapor, only $\approx 10\%$ of it is transported inland to generate precipitation, while rest of the moisture precipitates over the ocean during its transit (Oki and Kanae, 2006; Shiklomanov, 1998).

1

Measurements of the isotope composition of water in the various reservoirs of the hydrological cycle operating over the oceans is useful to infer information about the origin of water masses and understanding the formation mechanisms, transport pathways and finally the precipitation processes (Craig, 1961; Dansgaard, 1964; Yoshimura, 2015; Gat, 1996; Araguás-Araguás et al., 2000; Noone and Sturm, 2010; Gat et al., 2003; Benetti et al., 2014; Galewsky et al., 2016). Comparatively large volume of data exists over land to understand the terrestrial hydrological cycle, through the Global Network in Precipitation (GNIP) initiative of the International Atomic Energy Agency (IAEA). However, only a handful records on the spatial and temporal variability of precipitation and vapor isotopic composition over the oceans is available for any assessment (e.g. the Indian Ocean and the Southern Ocean (Uemura et al., 2008; Rahul et al., 2018; Prasanna et al., 2018), the Atlantic Ocean (Benetti et al., 2017b, a, 2015) and Mediterranean Sea (Gat et al., 2003)). Hence, further effort is needed to enhance the spatial and temporal sampling coverage over the oceans.

The isotopic composition of vapor on top of a water body is governed by the factors: i) Thermodynamic equilibrium process for phase transformation at a particular temperature ii) Kinetic or non-equilibrium processes where role of relative humidity and wind is significant and iii) Large-scale transport and mixing: due to the movement of air parcels laterally and vertically. Craig and Gordon (1965) initially proposed a two-layer model to simulate the isotopic composition of evaporated (referred to as the Traditional Craig-Gordon model). Recently, Gonfiantini et al. (2018) put forward a modified version referred to as the Unified Craig-Gordon Model. Both of these models incorporate the equilibrium and kinetic processes to simulate the isotopic composition of evaporated moisture. However, in order to get a realistic picture of the hydrological cycle over the ocean, the horizontal transport/advective mixing is important and should be incorporated.

In this paper we present stable isotope ratios in water vapor and ocean surface water from different locations covering varied oceanic settings; i.e. tropical, subtropical and polar latitudes, with a large range in the sea surface temperature, relative humidity and wind speed. While the role of temperature dependent equilibrium fractionation is well understood, the role of kinetic processes is under debate and requires further scrutiny. The performance of these Craig-Gordon evaporation models to simulate the isotopic composition of evaporation flux is evaluated along the sampling transect for different molecular diffusivity ratios and different fractions of molecular vs turbulent diffusion in the framework of the global closure assumption. The evaporation flux by the Craig-Gordon models is calculated assuming the 'global closure' i.e. the isotopic composition of atmospheric vapor is equal to the isotopic composition of evaporation. The models and the conditions that best match with the observations are identified, which are then used to calculate the local evaporation flux. This as done in the context of estimating the contribution of advected vs in-situ derived vapor along the sampling transect assuming a complete mixing of the advected and the locally generated vapor in the sampled water vapor in our study.

2   Methods

2.1   Sampling, isotopic analysis and meteorological parameters

The samples (water vapor, and surface water) for this study were collected along the stretch from Mauritius to Prydz Bay (24°S to 69°S and 57°E to 76°E) during two successive austral summers (January 2017 (SOE-IX) and December 2017 to January

2018 (SOE-X)) onboard the ocean research vessel SA Agulhas. The water vapor sampling inlet was set at ≈ 15m above the sea level. An aggregate of 71 water vapor samples were collected during the two expeditions. Fig. 1 shows the water vapor sampling locations. Alongside water vapor, 49 surface water samples were also collected. The details about the sampling procedures for collection of water vapor and surface water samples are given in the supplementary document. All these subjected to isotopic analysis using Finnigan Gasbench peripheral connected with an isotope ratio mass spectrometer (ThermoScientific MAT 253) (details are provided in the supplementary document). The isotope ratios are expressed in ‰ using the standard δ notation relative to Vienna Standard Mean Ocean Water (VSMOW).

In addition to water sampling, relative humidity (h), wind speed (ws), air temperature (Ta), sea surface temperature (SST), and atmospheric pressure (P) was recorded continuously during the expedition. Fig. 2 shows the latitudinal variation of these meteorological parameters. A wide range of these physical conditions are encountered since the sampling encompasses a large latitudinal transect.

2.2 Backward air-mass trajectories

In order to reconstruct the vertical profile of the atmospheric moisture transport along the sampling transect, backward air mass trajectories were generated using the Hybrid Single Particle Lagrangian Integrated Trajectory (HYSPLIT) model (Draxler and Hess, 1998; Stein et al., 2015) of NOAA-NCEP/NCAR forced with the Reanalysis data (Kanamitsu et al., 2002). HYSPLIT is a computational model hybrid between Lagrangian and Eulerian methods which generates the paths traversed by the air parcels and calculates meteorological variables such as temperature, relative humidity, specific humidity, rainfall, pressure etc. along the route. Back trajectories for 3 days are extracted since the average residence time of atmospheric moisture over the oceans is ≈3 days Trenberth (1998); Van Der Ent and Tuinenburg (2017). Figure 3 shows the back trajectories for the water vapor sampling locations. The sampling locations can be broadly categorized into zones which are defined by different wind patterns (i.e. velocity and the moisture carrying capacity). Westerlies and polar easterlies were identified based these 72 hour back-trajectories constructed at three different heights above the ocean surface. During the SOE X expedition, the change in trajectories to westerlies was at ≈31°S. At ≈63°S, change from westerlies to polar easterlies is seen. For SOE IX the transition from the westerlies to easterlies and then to polar westerlies was documented at the ≈33°S and ≈64°S latitudes respectively.

2.3 The Craig-Gordon Models

Craig-Gordon in 1965 (CG) Craig and Gordon (1965) proposed the first theoretical model to explain the isotopic composition of water vapor during the evaporation process. The isotopic composition of vapor generated on top of the ocean water depends on the isotopic composition of the surface oceanic water, the isotopic composition of water vapor in the ambient atmosphere along with the relative humidity at the site of sample collection. The interplay of equilibrium and kinetic fractionation between these phases governs the final isotopic composition in the water vapour and liquid. The equilibrium fractionation between ocean water and vapor is controlled by the sea surface temperature (SST). In comparison, relative humidity and wind speed control the the kinetic fractionation through the combination of processes which include both molecular and turbulent diffusion. Molecular diffusion leads to isotopic fractionation between liquid and vapor whereas the turbulent diffusion is non-fractionating. To

estimate the isotopic composition of water vapor CG model invokes two-layers; a laminar layer above the air-water interface where the transport process is active via molecular diffusion and a turbulent layer above the laminar layer in which the molecular transfer is predominantly by the action of turbulent diffusion. Assuming there is no divergence/convergence of air mass over the oceanic atmosphere, the isotopic ratio of the evaporation flux is given as Craig and Gordon (1965) referred to as Traditional Craig-Gordon Model (TCG):

$$R_{ev} = \alpha_k . \frac{R_L . \alpha_{eq} - h . R_A}{1 - h} \tag{1}$$

Where R_L, R_A, h, α_k and α_{eq} are respectively, the isotopic composition of the liquid water, the isotopic composition environmental atmospheric moisture, relative humidity, the kinetic and the equilibrium fractionation factors. The TCG models in this form and with modifications have been employed in diverse applications and used in numerous studies. The 'global closure' i.e. assuming a steady state is achieved in which the isotopic composition of vapor removed from the system has the same composition as atmospheric vapor (Merlivat, 1978):

$$R_A = R_{ev} \tag{2}$$

the global closure assumption (Eq. 2), is substituted in Eq (1) to give;

$$R_{ev} = \alpha_k . \frac{R_L . \alpha_{eq} - h . R_{ev}}{1 - h} \tag{3}$$

$$R_{ev}(1 - h) = \alpha_k . [R_L . \alpha_{eq} - h . R_{ev}] \tag{4}$$

$$R_{ev}(1 - h) + \alpha_k h . R_{ev} = \alpha_k . R_L . \alpha_{eq} \tag{5}$$

$$R_{ev}[(1 - h) + \alpha_k . h] = \alpha_k . R_L . \alpha_{eq} \tag{6}$$

$$R_{ev} = \frac{\alpha_{eq} \alpha_k R_L}{(1 - h) + \alpha_k . h} \tag{7}$$

Recently, Gonfiantini et al. (2018) proposed a modified version of the model, termed as Unified Craig-Gordon (UCG) model in which the parameters controlling the isotopic composition of the evaporation flux are considered simultaneously. From Gonfiantini et al. (2018), the net evaporation rate of liquid water (E) is the difference between the vaporization rate, ψ_{vap}, and the atmospheric vapor capture rate (i.e; condensation) by the liquid water, ψ_{cap}.

$$E = \psi_{vap} - \psi_{cap} = (\gamma - h)\psi_{cap}^o \tag{8}$$

4

Where the ψ^o_{cap} is the vaporization rate of pure water, h is the relative humidity and γ is the thermodynamic activity coefficient of evaporating water which is <1 for the saline solutions and 1 for the pure water or dilute solutions.

From Eq. (8), We can write;

$$R_{ev}(\gamma - h)\Psi^o_{vap} = R_{esc}\gamma\Psi^o_{vap} - R_{cap}h\Psi^o_{vap} \tag{9}$$

$$R_{ev}(\gamma - h)\Psi^o_{vap} = \frac{R_L}{\alpha_{eq}\alpha^x_{diff}}\gamma\Psi^o_{vap} - \frac{R_A}{\alpha^x_{diff}}h\Psi^o_{vap} \tag{10}$$

$$R_{ev} = \frac{\frac{R_L}{\alpha_{eq}\alpha^x_{diff}}\gamma - \frac{R_A}{\alpha^x_{diff}}h}{\gamma - h} \tag{11}$$

Where R_L, R_{esc}, R_{cap} and R_A are, respectively the isotopic composition of the liquid water, isotopic composition of vapor escaping to the saturated layer above which is in thermodynamic equilibrium with water, isotopic composition of environmental atmospheric moisture captured by the equilibrium layer and the isotopic composition environmental atmospheric moisture. R_L, R_{esc}, R_{cap} and R_A are defined as in Gonfiantini et al. (2018). α_{eq} is the isotopic fractionation factor between the liquid water and the vapor in the equilibrium layer. α_{diff} is the isotopic fractionation factor for diffusion in air affecting the vapor escaping from the equilibrium layer and the environmental vapor entering the equilibrium layer; x is the turbulent index of atmosphere. Introducing the global closure assumption, Eq. (2) in Eq. (11) gives:

$$R_{ev} = \frac{\frac{R_L}{\alpha_{eq}\alpha^x_{diff}}\gamma - \frac{R_{ev}}{\alpha^x_{diff}}h}{\gamma - h} \tag{12}$$

$$R_{ev}(\gamma - h) = \frac{R_L}{\alpha_{eq}\alpha^x_{diff}}\gamma - \frac{R_{ev}}{\alpha^x_{diff}}h \tag{13}$$

$$R_{ev}(\gamma - h) + \frac{R_{ev}}{\alpha^x_{diff}}h = \frac{R_L}{\alpha_{eq}\alpha^x_{diff}}\gamma \tag{14}$$

$$R_{ev}[(\gamma - h) + \frac{h}{\alpha^x_{diff}}] = \frac{R_L}{\alpha_{eq}\alpha^x_{diff}}\gamma \tag{15}$$

$$R_{ev}[\frac{(\gamma - h)\alpha^x_{diff} + h}{\alpha^x_{diff}}] = \frac{R_L}{\alpha_{eq}\alpha^x_{diff}}\gamma \tag{16}$$

$$R_{ev} = \frac{R_L}{\alpha_{eq}\alpha^x_{diff}}\gamma[\frac{\alpha^x_{diff}}{(\gamma - h)\alpha^x_{diff} + h}] \tag{17}$$

5

$$R_{ev} = \frac{R_L \gamma}{\alpha_{eq}[\alpha_{diff}^x(\gamma - h) + h]} \tag{18}$$

The temperature dependent equilibrium fractionation factor is calculated using the formulation given by (Horita and Wesolowski, 1994). The kinetic factor takes into account diffusion in air affecting the vapor escaping from the equilibrium layer and is controlled by α_{diff}, which is the molecular diffusivity of the different isotopologues of water. Molecular diffusivities (α_{diff}^O, α_{diff}^H) data are taken from three previous studies Merlivat (1978) (1.0285, 1.0251), Cappa et al. (2003) (1.0318, 1.0164) and Pfahl and Wernli (2009) (1.0076, 1.0039) referred to as MJ, CD and PW respectively. x is the turbulence index of atmosphere which signifies the proportion of vapor that escapes by isotopic fractionating molecular diffusion and non-fractionating turbulent diffusion. When x = 1 the vapor escapes solely by molecular diffusion and for x = 0 the vapor escapes only due to turbulent diffusion.

3 Results

3.1 Isotopic measurements along the transect

$\delta^{18}O$ of surface water was > 0 ‰ until $\approx 40°$S latitude. A transition to lighter isotopic composition was observed beyond $\approx$ 45°S latitude with a drop documented in the surface water isotopic values on approaching the coastal Antarctic regions. Figure 4a shows the latitudinal variation of $\delta^{18}O_{sw}$, plotted along with salinity values measured along the transect. In addition, the $\delta^{18}O$ of ocean surface water extracted from the Global Sea Water 18O Database (SWD) (Schmidt et al., 1999) are also plotted. There is a mismatch between the observed depleted isotopic values near coastal Antarctica with SWD values. The SWD is a surface interpolated dataset based on point observations in the global ocean. This is probably one of the major causes of the difference, the others being the season or the month of sample collection.

The $\delta^{18}O_{wv}$ and δ^2H_{wv} in water vapor samples showed a consistent trend across latitude for both the expeditions. The $\delta^{18}O_{wv}$ (δ^2H_{wv}) of water vapor varies from -10.9‰ (-80.8‰) to -27.5‰(-221.4‰) respectively. The vapor isotopic composition is seen to be gradually decreasing with lighter isotopic values at higher latitudes. A steady drop was noted from $\approx$30°S to $\approx$65°S and a sharp change in the gradient was registered at $\approx$65°S. Extreme lighter values recorded on approaching $\approx$65°S are attributed to factors such as low temperature and the mixing of lighter vapor from continental Antarctica (Uemura et al., 2008). There are deviations from this general trend with heavier isotopic composition observed at the higher latitudes or vice versa. These variations can be accounted, by taking into consideration the source and the path of air masses. The lighter (heavier) values of vapor isotopic composition can be traced to the source being lower (higher) latitudes.

Deuterium excess (d-excess or dxs), defined as $d - excess = \delta^2H - 8 \times \delta^{18}O$, is a second order isotope parameter which is a measure of kinetic fractionation during evaporation (Dansgaard, 1964). d-excess in the water vapor correlates with meteorological parameters at the ocean surface such as relative humidity, sea surface temperature and wind speed (Uemura et al., 2008; Rahul et al., 2018; Benetti et al., 2014; Midhun et al., 2013). Therefore, it serves as a proxy for the moisture source conditions in the evaporation regions. The dxs and relative humidity are strongly coupled, which is determined by the magnitude of

moisture gradient between evaporating water surface and overlying unsaturated air. In other words, lower the relative humidity higher is the dxs in the overlying moisture. Wind speed regulates the turbulent vs molecular diffusion across the diffusive layer. The role of SST in governing the dxs is through the process of equilibrium fractionation, which is temperature dependent. The dxs values in water vapor samples range from 18.7‰ to -23.7‰. A relatively higher dxs values in the water vapor from $\approx 25°$S to $\approx 45°$S with a slight step change to lower dxs values was recorded on approaching 45°S which extends until $\approx 65°$S. Beyond $\approx 65°$S a slight increment in the vapor dxs was observed. The very low dxs values due to mixing of vapor evaporated from sea-spray under high wind speed conditions are observed during the passage of extra-tropical cyclones. The statistics of the isotopic composition of water vapor are tabulated in Table 1.

3.2 Meteorological controls on the isotopic composition of water vapor

The $\delta^{18}O_{wv}$ and $\delta^2 H_{wv}$ are positively correlated with SST, negatively correlated with wind speed and uncorrelated with relative humidity. For all the water vapor samples, $\delta^2 H_{wv}$ and $\delta^{18}O_{wv}$ are correlated with SST explaining $\approx 33\%$ of the variance in $\delta^{18}O_{wv}$ and $\approx 50\%$ of the variance in $\delta^2 H_{wv}$. The correlation coefficient is higher if sampling from individual years is considered separately. In all cases, the slope and intercept of the regression equation between the isotopic composition of water vapor and SST is comparable with previous observations from the Southern Ocean Uemura et al. (2008). The linear regression plots are shown Figure 5 and the regression parameters (slope, intercept, standard errors and r^2) for $\delta^{18}O$ and $\delta^2 H$ are listed in Table 1.(S) and Table 2.(S) respectively. The regression equations are calculated for different sample classifications, with and without the influence of Antarctic vapor mixing as evident from the back trajectories (i.e. samples collected north of 65°S) and for individual expeditions.

Figure 6 shows the regression plots of dxs in vapor with the meteorological conditions and the parameters defining the regression equations are listed in Table 2. For samples collected north of 65°S, the linear regression equation describing the relationship between dxs and relative humidity is dxs=-0.56h+46.36 (r^2=0.49). These slope and intercept values are similar to the earlier records, documenting the isotope variability in water vapour from the Southern Ocean (Uemura et al., 2008; Rahul et al., 2018) the Bay of Bengal (Midhun et al., 2013), the Atlantic (Benetti et al., 2014) and the Mediterranean (Gat et al., 2003). For samples collected south of 65°S the relationship becomes weaker. The strength of the dxs vs h relationship was stronger if data exclusively from the expeditions is considered separately, for the SOE IX and SOE X as dxs=-0.64h+57.4 (r^2=0.77) and dxs=-0.64h+48.7 (r^2=0.61) respectively. Collectively for both the expeditions, the dxs in vapor is positively correlated with the SST and the regression parameters are comparable with those from previous observations in the Southern Ocean and also for the Atlantic Ocean and the Bay of Bengal. For SST vs dxs, the linear regression equation for samples collected north of 65°S is given by dxs=0.70sst-4.65 (r^2=0.49). The dxs of water vapor samples are negatively correlated with wind speed. For samples collected north of 65°S the correlation the regression equation is given by dxs=-0.53ws+11.65 (r^2=0.23). Our observation is consistent with the earlier studies suggesting the dependency of water vapor d-excess on relative humidity, SST and wind speed.

4 Discussion

4.1 Craig-Gordon (CG) model evaluation

The isotopic composition of evaporation flux from the oceans is calculated using the CG models (TCG and UCG) assuming three molecular diffusivity ratios driving the kinetic fractionation and for varied contribution of turbulent vs molecular diffusion enabled transport factors. The simulated values of the isotopic composition of evaporation flux with these different models under the global closure assumption are compared with the measured isotopic values of water vapor over the ocean. The model and the constraints that best describe the observations are selected based on the model predicted and observed relationships between the dxs of water vapor and physical parameters (SST, ws and h).

The TCG and the UCG models are run for MJ, CD and PW molecular diffusivities and for the turbulence index of the atmosphere varying from 0-1 with an increment of 0.1. Figure 7 and Figure 8 shows the comparison between the TCG and UCG modelled vapor isotopic composition ($\delta^{18}O$ and d-excess) with the observations. There are values for the turbulence index (x) of the atmosphere where model predicted $\delta^{18}O$ and d-excess overlap with the observations for both TCG and UCG models with MJ and CD molecular diffusivity ratios. However, there is a clear mismatch between the model predicted $\delta^{18}O$ and d-excess for the recommended PW molecular diffusivities in both UCG and TCG models. Another noteworthy feature of the plots is the for all the model runs a large difference is seen between the modelled and observed isotopic composition for water vapor samples collected south of $\approx 65°S$ latitudes and the best match is seen for samples collected North of $\approx 65°S$. This difference is attributed to the advection and mixing of lighter Antarctic moisture to local moisture for samples collected beyond $\approx 65°S$.

To evaluate the performance of the prediction by these models and identify the parameters that best describe the observations, the slope of the dxs vs relative humidity predicted by the different model runs are compared with the observed relationships documented based on actual data on samples collected north of 65°S. Figure 1.(S) depicts the comparison between the observed and the model predicted relationships. The UCG models and the parameters that match the observed slope of the relative humidity vs d-excess relationship (-0.56 ± 0.08) are $UCG_{x=0.8}^{MJ}$, $UCG_{x=0.6}^{CD}$ and $UCG_{x=0}^{PW}$. Similarly for the TCG models $TCG_{x=0.6}^{MJ}$, $TCG_{x=0.7}^{CD}$ and $TCG_{x=0}^{PW}$ predict the slopes that are comparable with the observed value. The $\delta^{18}O$ and d-excess of predicted by these models are plotted with the observations in Figure 9.

The consistency of model results and observations are best described using a linear regression equation which links model predicted d-excess and the meteorological parameters (relative humidity, sea surface temperature and wind speed). These regression plots are displayed in Figure 2.(S). The difference between the model predicted and the observed values of slopes and intercepts are shown in Figure 10. The largest difference between the observed and model predicted slopes are intercepts are for the PW molecular diffusivities for both UCG and the TCG models and therefore excluded from further discussion. For the dxs vs relative humidity relationship, $UCG_{x=0.8}^{MJ}$ and $UCG_{x=0.6}^{CD}$ show the smallest difference between the observed and modelled slopes and intercepts followed by $TCG_{x=0.6}^{MJ}$ and $TCG_{x=0.7}^{CD}$. In case of dxs vs SST relationship, 'the TCG models show the least difference between the slopes and the UCG model predicts the intercept values that are consistent with the observations. Similarly, for the and dxs vs ws relationships, the UCG and the TCG models produce the values that predict the

8

slope and the intercept values with the least deviation from the observed values. The models that best describe the slope and intercept values of linear regression equation defining the d-excess vs the meteorological parameters, the root mean square error of the modelled vs observed $\delta^{18}O$ and d-excess are listed in Table 3. The ability of the models to predict the $\delta^{18}O$ and d-excess are better demonstrated by the water vapor samples which were collected north of 65°S. The models predict the d-excess with a better correlation than $\delta^{18}O$ and the TCG model show a slightly higher possibility to predict the d-excess values than the UCG model.

4.2 Understanding the equilibrium/disequilibrium

The isotopic composition of water vapor over the ocean is governed by the equilibrium and kinetic processes which are defined by the meteorological condition. However, considering only these factors is insufficient to explain the observed variation in the isotopic composition of vapor on top of the ocean. Advective mixing of transported vapor to the locally generated vapor is important and needs to be taken into consideration. Fig. 11a shows the difference between the $\delta^{18}O$ and $\delta^2 H$ isotopic composition of vapor (at equilibrium with ocean surface water) and the observed vapor isotopic composition. Kinetic fractionation can explain a part of the departure from the equilibrium state and is evaluated based on the Craig-Gordon models as described in the previous section ($E_{UCG}^{MJ,0.8}$, $E_{UCG}^{CD,0.6}$, $E_{TCG}^{MJ,0.6}$ and $E_{TCG}^{CD,0.7}$). The difference between isotopic composition of equilibrium vapor ($\delta^{18}O$ and $\delta^2 H$) and the modelled isotopic composition by the E_{UCG}, E_{TCG} is also plotted in Figure 11b-e. In order to calculate the fractional contribution of the local and advected moisture along the sampling transect, a two component mixing framework is invoked. The local end member is based on the isotopic composition of vapor predicted by the best match UCG and the TCG model predicted parameters. The calculations are done assuming the isotopic composition of the advected vapor due to westerlies similar to the earlier proposition (Uemura et al., 2008) ($\delta^2 H \approx$-109‰) in the region between 31°S to 65°S. For samples collected in the polar ocean south of 65°S, the temperature plays the role of limiting the local evaporation process and hence the large differences from the equilibrium conditions can be explained by invoking the process of mixing of Antarctic vapor which is transported to this region by the interplay of polar easterlies. The average isotopic composition of water vapor collected at Dome C site (Dec 2014-Jan) (Wei et al., 2019) ($\delta^2 H$= -490±23‰) is chosen as representative of the advected vapor transported by the polar easterlies. It is seen that in order to explain the water vapor isotope ratio observation over the ocean south of 65°S, the contribution of lighter Antarctic vapor is expected. Fig. 12b shows the relative contribution of advected and locally generated moisture in our observation. The advected component is a prominent component of the ambient vapor on approaching higher latitudes. South of 65°S the amount of moisture present in the atmosphere is less and is largely local in origin with a small mixing of lighter Antarctic vapor. However, the contribution of the Antarctic vapor linearly increases on approaching the coastal regions.

5 Conclusions

In this study, the isotopic composition of water vapor and surface water samples collected across a latitudinal transect from Mauritius to Prydz in the Southern Ocean are described. The isotopic composition of evaporating vapor is governed by the iso-

topic composition of the water, ambient vapor isotopic composition, exchange and mixing processes at the water-air interface as well as the local meteorological conditions. These controlling parameters were considered separately or simultaneously for explaining the observation best quantifying the evaporation mechanism adopted in the Craig-Gordon models. The Traditional Craig-Gordon (Craig and Gordon, 1965) (TCG) and the Unified Craig-Gordon (UCG) (Gonfiantini et al., 2018) equations were used to predict the isotopic composition of evaporation flux after incorporating different molecular diffusivity ratios at varying fractions of molecular and turbulent diffusion. The best match for between the modelled and observed values is seen by using the MJ and CD molecular diffusivity ratios whereas the largest mismatch is for the PW values of the molecular diffusivities. The results ascertain the importance of the fraction of molecular vs turbulent fraction (i.e. isotopically fractionating vs non fractionating exchange) used to predict the isotopic composition of the evaporation flux in these Craig-Gordon models. $UCG_{x=0.8}^{MJ}, UCG_{x=0.6}^{CD}, TCG_{x=0.6}^{MJ}$ and $TCG_{x=0.7}^{CD}$ models predicted the slope and the intercepts of dxs vs meteorological parameters with an appreciable accuracy and consistent with the observations. The remaining difference between the observed and simulated isotopic composition of water vapor is explained by incorporating an advective framework where the advected vapor mass is assumed to mix with the locally generated vapor in a mixing model. The assignment of the advective component is based on the path followed by the air-masses calculated by the HYSPLIT trajectory model. The relative contribution of advected and locally evaporated fluxes was estimated by assigning end member isotopic composition and solving in a two-component mixing framework. The approximation of the locally generated end member composition is based on $UCG_{x=0.8}^{MJ}, UCG_{x=0.6}^{CD}, TCG_{x=0.6}^{MJ}$ and $TCG_{x=0.7}^{CD}$. The advected moisture flux is assigned values based on the origin and path followed by the back trajectories. It is found that beyond 65°S latitude lighter isotope values observed in the water can be explained by invoking mixing of Antarctic vapor with its contribution linearly increasing towards the coast.

Although the advective model can explain the water vapor composition along the transect, nonetheless there can be other sources of advective humidity to the surface layers such as from upper atmospheric layers with different properties, vapor generated from the re-evaporation of rainfall, evaporation of sea spray or sublimation of snow and ice. These processes may occur under conditions which are not possible to take into account due the cryogenic sampling method for collection of water vapor. The study can be improved by measuring the water vapor isotopic composition continuously along the transect using a cavity ring down spectrometry and high resolution precipitation collection during the passage of extra-tropical cyclones.

Author contributions

SSD and PG conceptualized the study. SSD and AS performed the sample collection and analysis. SSD wrote the paper and PG supervised the study. AK provided the resources during the expeditions.

Data Availability

The data that support the findings of this study have been uploaded as a supplementary document.

Declaration of interests

The authors declare that they have no known competing financial interests or personal relationships that could have appeared to influence the work reported in this paper.

11

References

Araguás-Araguás, L., Froehlich, K., and Rozanski, K.: Deuterium and oxygen-18 isotope composition of precipitation and atmospheric moisture, Hydrological Processes, 14, 1341–1355, 2000.

305 Benetti, M., Reverdin, G., Pierre, C., Merlivat, L., Risi, C., Steen-Larsen, H. C., and Vimeux, F.: Deuterium excess in marine water vapor: Dependency on relative humidity and surface wind speed during evaporation, Journal of Geophysical Research: Atmospheres, 119, 584–593, 2014.

Benetti, M., Aloisi, G., Reverdin, G., Risi, C., and Sèze, G.: Importance of boundary layer mixing for the isotopic composition of surface vapor over the subtropical North Atlantic Ocean, Journal of Geophysical Research: Atmospheres, 120, 2190–2209, 2015.

310 Benetti, M., Reverdin, G., Aloisi, G., and Sveinbjörnsdóttir, Á.: Stable isotopes in surface waters of the Atlantic Ocean: Indicators of ocean-atmosphere water fluxes and oceanic mixing processes, Journal of Geophysical Research: Oceans, 122, 4723–4742, 2017a.

Benetti, M., Steen-Larsen, H. C., Reverdin, G., Sveinbjörnsdóttir, Á. E., Aloisi, G., Berkelhammer, M. B., Bourlès, B., Bourras, D., De Coetlogon, G., Cosgrove, A., et al.: Stable isotopes in the atmospheric marine boundary layer water vapour over the Atlantic Ocean, 2012–2015, Scientific data, 4, 160 128, 2017b.

315 Cappa, C. D., Hendricks, M. B., DePaolo, D. J., and Cohen, R. C.: Isotopic fractionation of water during evaporation, Journal of Geophysical Research: Atmospheres, 108, 2003.

Chahine, M. T.: The hydrological cycle and its influence on climate, Nature, 359, 373, 1992.

Craig, H.: Isotopic variations in meteoric waters, Science, 133, 1702–1703, 1961.

Craig, H. and Gordon, L. I.: Deuterium and oxygen 18 variations in the ocean and the marine atmosphere, 1965.

320 Dansgaard, W.: Stable isotopes in precipitation, Tellus, 16, 436–468, 1964.

Draxler, R. R. and Hess, G.: An overview of the HYSPLIT_4 modelling system for trajectories, Australian meteorological magazine, 47, 295–308, 1998.

Galewsky, J., Steen-Larsen, H. C., Field, R. D., Worden, J., Risi, C., and Schneider, M.: Stable isotopes in atmospheric water vapor and applications to the hydrologic cycle, Reviews of Geophysics, 54, 809–865, 2016.

325 Gat, J., Klein, B., Kushnir, Y., Roether, W., Wernli, H., Yam, R., and Shemesh, A.: Isotope composition of air moisture over the Mediterranean Sea: an index of the air–sea interaction pattern, Tellus B, 55, 953–965, 2003.

Gat, J. R.: Oxygen and hydrogen isotopes in the hydrologic cycle, Annual Review of Earth and Planetary Sciences, 24, 225–262, 1996.

Gonfiantini, R., Wassenaar, L. I., Araguas-Araguas, L., and Aggarwal, P. K.: A unified Craig-Gordon isotope model of stable hydrogen and oxygen isotope fractionation during fresh or saltwater evaporation, Geochimica et Cosmochimica Acta, 235, 224–236, 2018.

330 Horita, J. and Wesolowski, D. J.: Liquid-vapor fractionation of oxygen and hydrogen isotopes of water from the freezing to the critical temperature, Geochimica et Cosmochimica Acta, 58, 3425–3437, 1994.

Kanamitsu, M., Ebisuzaki, W., Woollen, J., Yang, S.-K., Hnilo, J., Fiorino, M., and Potter, G.: Ncep–doe amip-ii reanalysis (r-2), Bulletin of the American Meteorological Society, 83, 1631–1643, 2002.

Korzoun, V. and Sokolov, A.: World water balance and water resources of the earth, Water Development, Supply and Management (UK)(USA)(Canada)(Australia)(France)(Germany, FR), 1978.

335 Merlivat, L.: Molecular diffusivities of $H_2^{16}O$, $HD^{16}O$, and $H_2^{18}O$ in gases, The Journal of Chemical Physics, 69, 2864–2871, 1978.

Midhun, M., Lekshmy, P., and Ramesh, R.: Hydrogen and oxygen isotopic compositions of water vapor over the Bay of Bengal during monsoon, Geophysical Research Letters, 40, 6324–6328, 2013.

Noone, D. and Sturm, C.: Comprehensive dynamical models of global and regional water isotope distributions, in: Isoscapes, pp. 195–219, Springer, 2010.

Oki, T. and Kanae, S.: Global hydrological cycles and world water resources, science, 313, 1068–1072, 2006.

Pfahl, S. and Wernli, H.: Lagrangian simulations of stable isotopes in water vapor: An evaluation of nonequilibrium fractionation in the Craig-Gordon model, Journal of Geophysical Research: Atmospheres, 114, 2009.

Prasanna, K., Ghosh, P., Bhattacharya, S., Rahul, P., Yoshimura, K., and Anilkumar, N.: Moisture rainout fraction over the Indian Ocean during austral summer based on 18O/16O ratios of surface seawater, rainwater at latitude range of 10 N-60 S., Journal of Earth System Science, 127, 2018.

Rahul, P., Prasanna, K., Ghosh, P., Anilkumar, N., and Yoshimura, K.: Stable isotopes in water vapor and rainwater over Indian sector of Southern Ocean and estimation of fraction of recycled moisture, Scientific reports, 8, 2018.

Schmidt, G., Bigg, G., and Rohling, E.: Global seawater oxygen-18 database–v1. 21, Online at http://data. giss. nasa. gov/o18data, online at http://data. giss. nasa. gov/o18data, 1999.

Shiklomanov, I. A.: World water resources: a new appraisal and assessment for the 21st century: a summary of the monograph World water resources, Unesco, 1998.

Stein, A., Draxler, R., Rolph, G., Stunder, B., Cohen, M., and Ngan, F.: NOAA's HYSPLIT atmospheric transport and dispersion modeling system, Bulletin of the American Meteorological Society, 96, 2059–2077, 2015.

Trenberth, K. E.: Atmospheric moisture residence times and cycling: Implications for rainfall rates and climate change, Climatic change, 39, 667–694, 1998.

Uemura, R., Matsui, Y., Yoshimura, K., Motoyama, H., and Yoshida, N.: Evidence of deuterium excess in water vapor as an indicator of ocean surface conditions, Journal of Geophysical Research: Atmospheres, 113, 2008.

Van Der Ent, R. J. and Tuinenburg, O. A.: The residence time of water in the atmosphere revisited, Hydrology and Earth System Sciences, 21, 779–790, 2017.

Wei, Z., Lee, X., Aemisegger, F., Benetti, M., Berkelhammer, M., Casado, M., Caylor, K., Christner, E., Dyroff, C., García, O., et al.: A global database of water vapor isotopes measured with high temporal resolution infrared laser spectroscopy, Scientific data, 6, 180 302, 2019.

Yoshimura, K.: Stable water isotopes in climatology, meteorology, and hydrology: A review, Journal of the Meteorological Society of Japan. Ser. II, 93, 513–533, 2015.
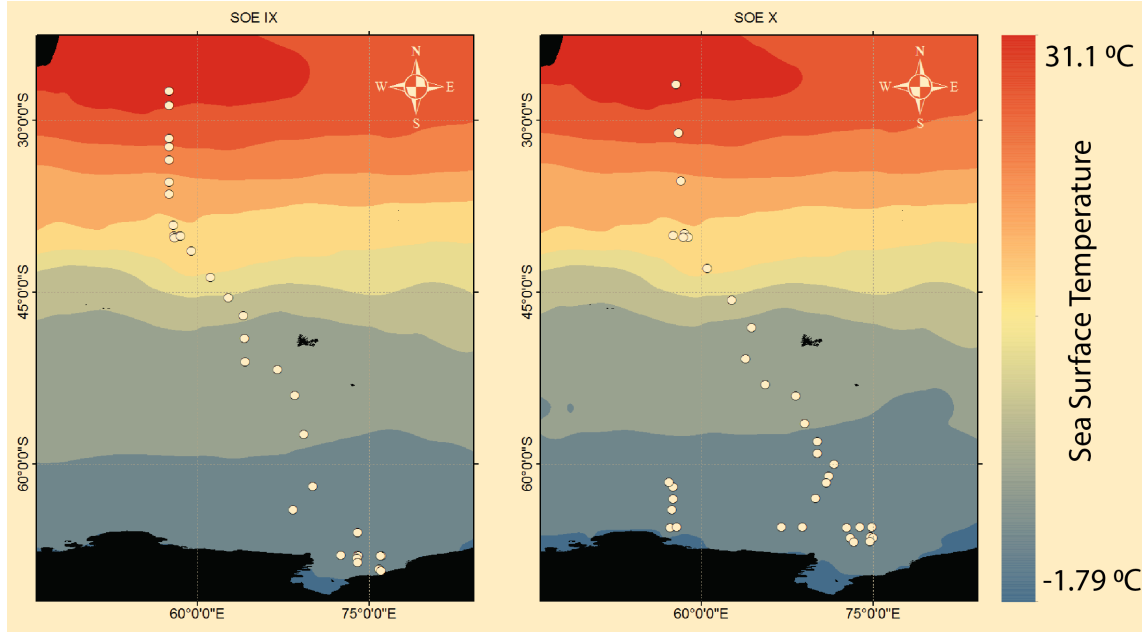
Figure 1. The water vapor sampling locations during the two expeditions (January 2017 (SOE-IX) and December 2017 to January 2018 (SOE-X)) shown as open circles overlain on the map of mean monthly sea surface temperature during the two expeditions. The sea surface temperature data is from Reanalysis dataset Kanamitsu et al. (2002).

Table 1. Descriptive statistics of the water vapor isotopic composition.

	$\delta^{18}O(‰)$	$\delta^2H(‰)$	**d-excess**$(‰)$
SOE IX Water Vapor(n=34)			
Max	-10.86	-80.79	18.65
Min	-27.47	-221.38	-8.37
Mean(Stdev)	-16.96(±5.25)	-130.35(±44.43)	5.35(±8.06)
SOE X Water Vapor(n=37)			
Max	-11.46	-88.03	14.54
Min	-21.18	-163.28	-23.71
Mean(Stdev)	-15.77(±2.53)	-126.07(±20.23)	0.08(±8.46)
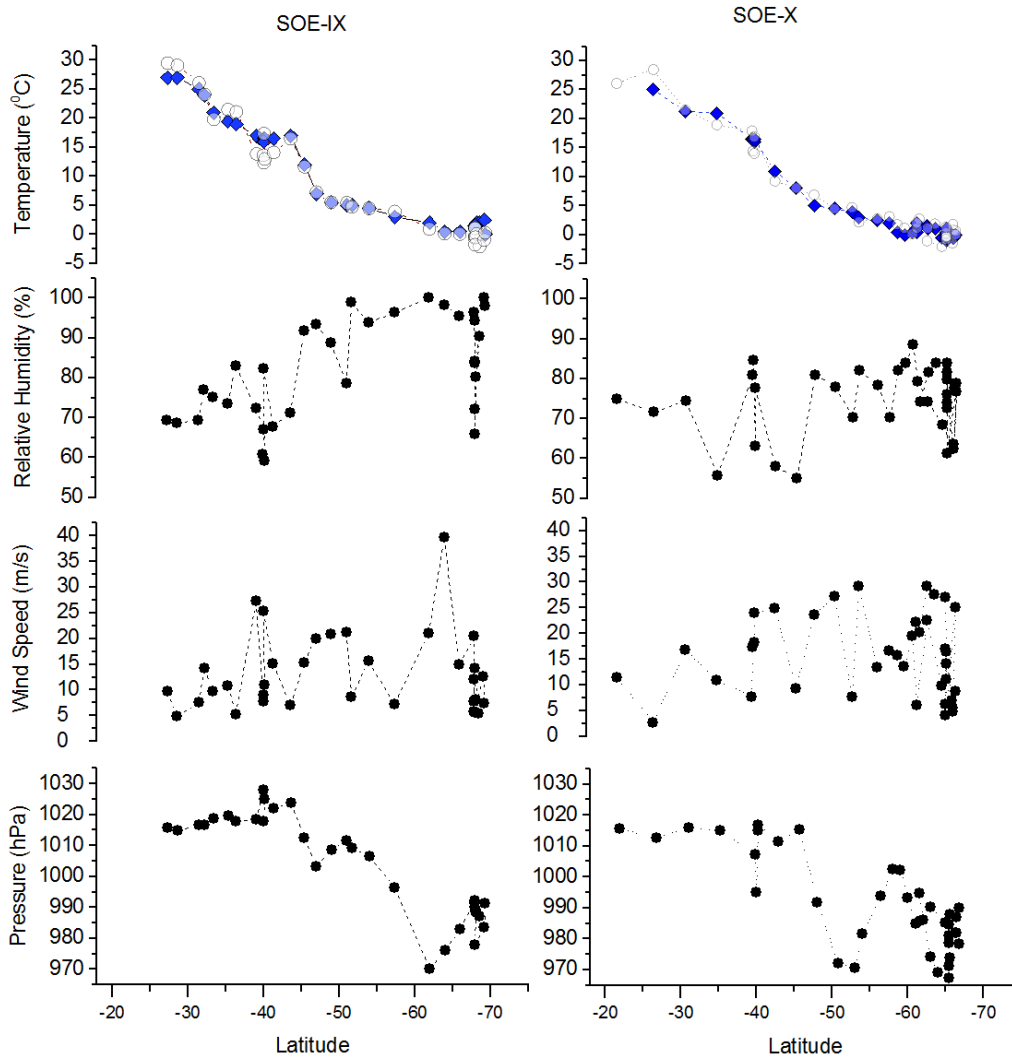
Figure 2. Latitudinal variability of measured meteorological parameters, temperature, relative humidity, wind speed and atmospheric pressure. Filled blue diamonds and open circles in the temperature plot represent the sea surface temperature and air temperature respectively.
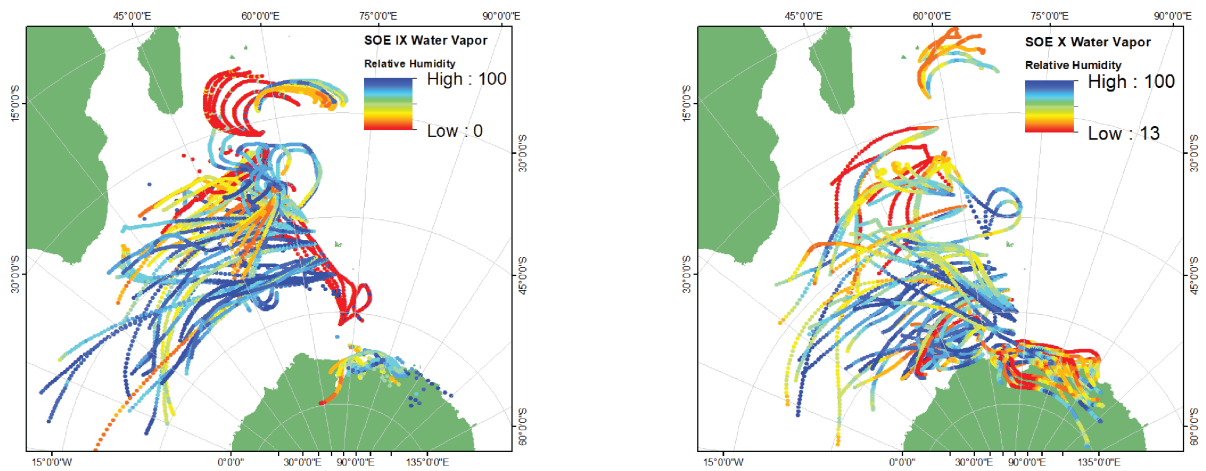
Figure 3. 72 hours back trajectories calculated using HYSPLIT with Reanalysis data as forcing. The trajectories shown are for three heights surface, 500m and 1500m above the mean sea level and the colors depict the variation of relative humidity along the trajectories.
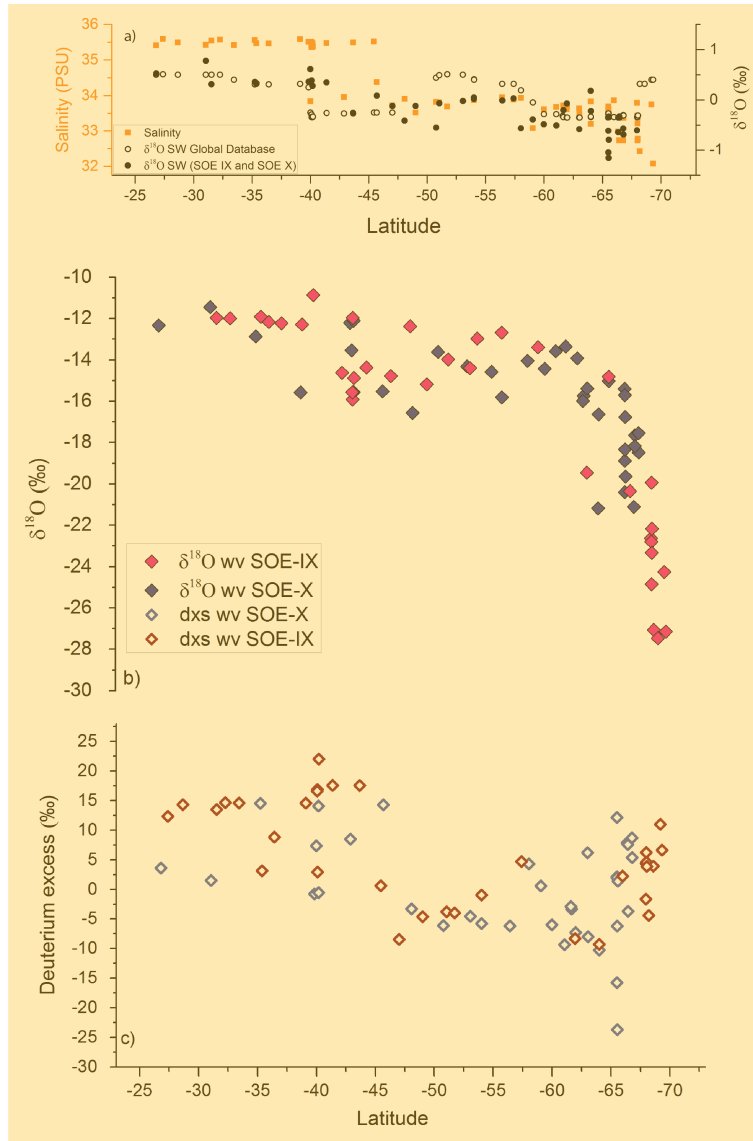
Figure 4. a) Measured $\delta^{18}O_{SW}$ as black filled circles and values of surface water isotopic composition extracted from the global sea water $\delta^{18}O_{SW}$ database along the latitudinal transect (open black circles). Also plotted as orange filled squares are the salinity values along the transect b) Pink and purple filled diamonds depict the $\delta^{18}O_{WV}$ of water vapor samples collected during the SOE-IX and SOE-X respectively at height of $\approx 15m$ above the water surface. c) latitudinal variation of dxs in water vapor samples shown as open red and purple diamonds for SOE-IX and SOE-X respectively.
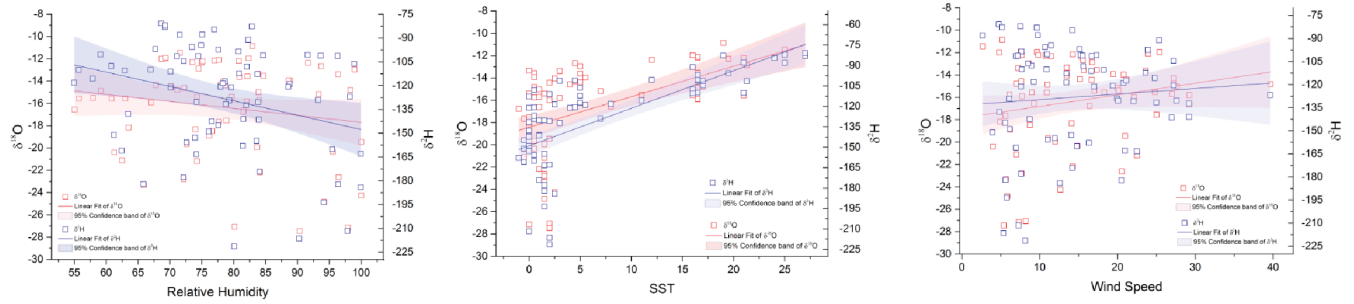
Figure 5. Linear regression for isotopic composition of water vapor and physical parameters(sea surface temperature, relative humidity and wind speed). Hollow red and blue squares represent the $\delta^{18}O$ and $\delta^2 H$ respectively and the shaded areas depict the 95% confidence bands. The linear regression lines are shown as blue and red for $\delta^2 H$ and $\delta^{18}O$ respectively. The slope and intercept of the linear regression equations along with data from Uemura et al. (2008) are listed in Table 1.(S) and Table 2.(S).
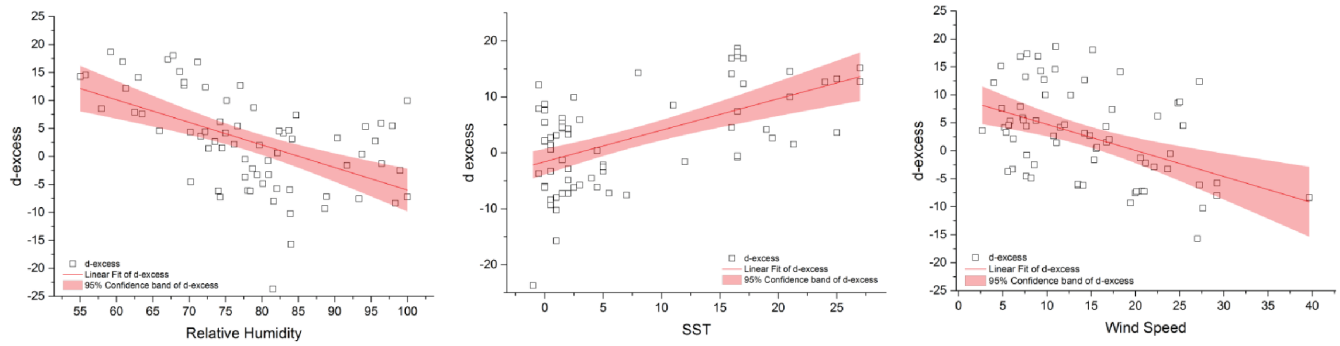
Figure 6. Regression plots for d-excess (hollow black squares) in water vapor and the meteorological conditions (relative humidity, sea surface temperature and wind speed). The shaded region depicts the 95% confidence bands of d-excess. The slope and intercept of the regression equations along with data from Uemura et al. (2008) are listed in Table 2.
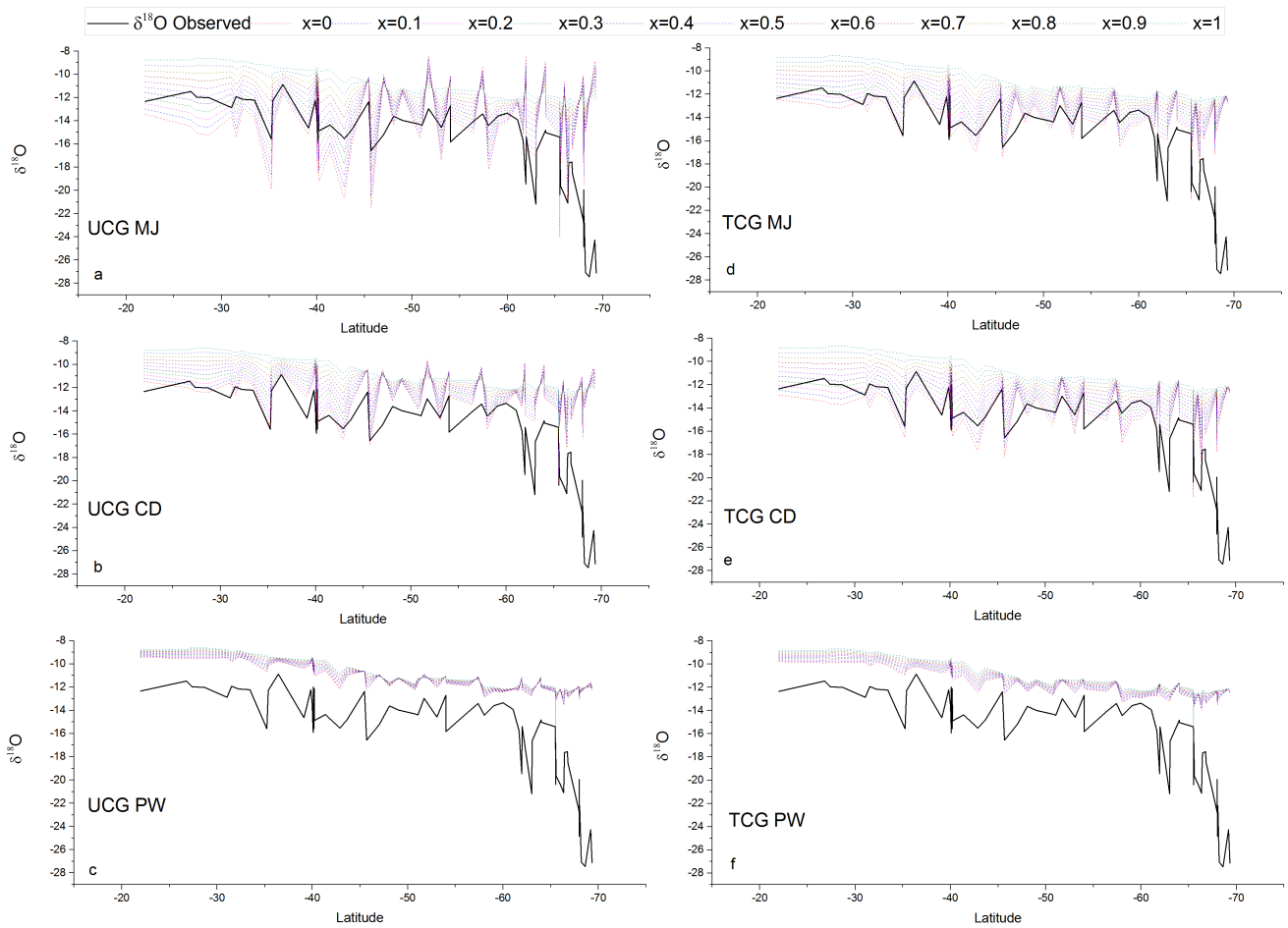
Figure 7. Comparison between the latitudinal distribution of the measured water vapor $\delta^{18}O$ (black lines) and that predicted by the TCG and UCG models, employing the global closure assumption for different molecular diffusivity ratios and turbulence indices, shown as colored lines.
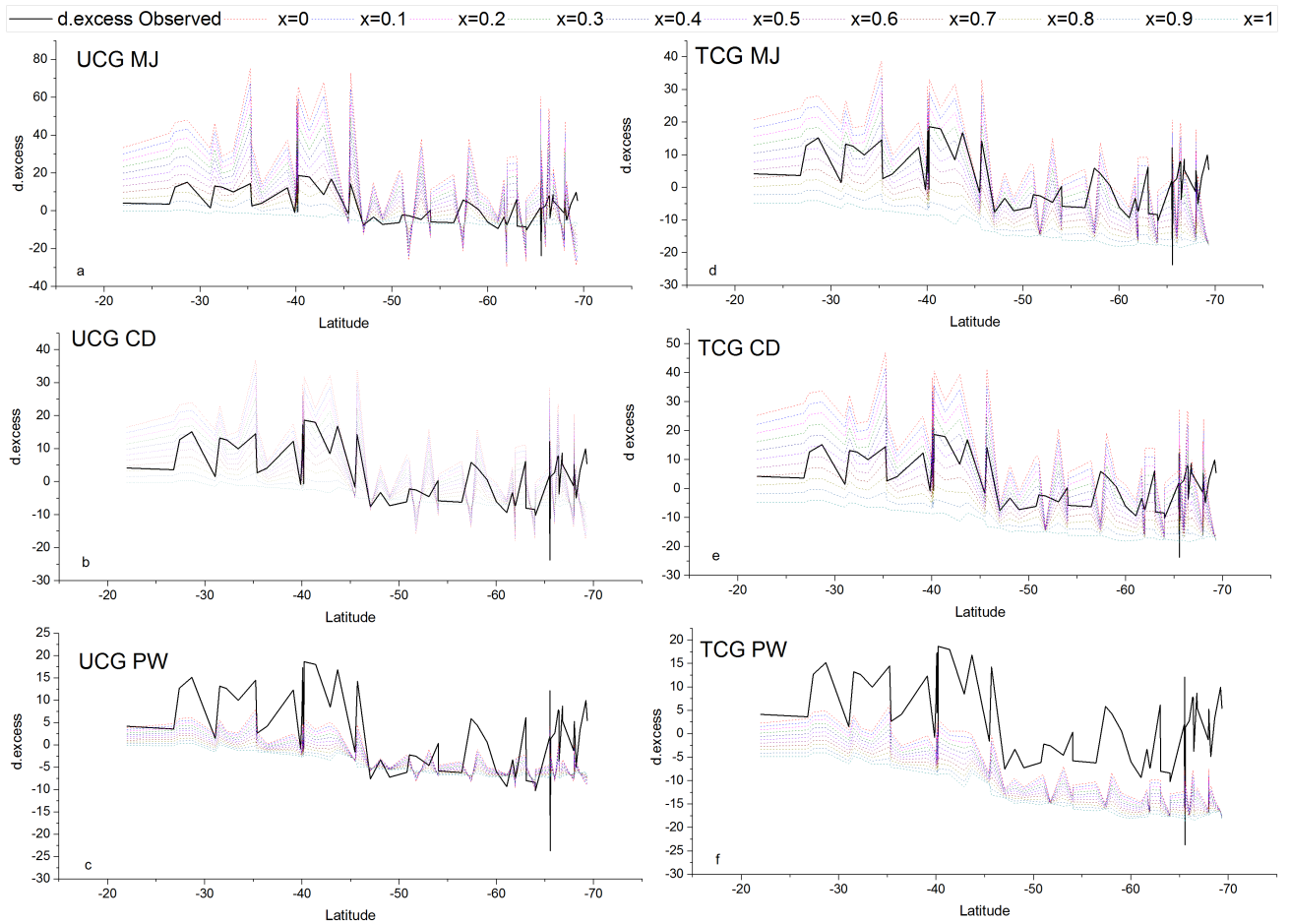
Figure 8. Comparison between the latitudinal distribution of the measured d-excess in water vapor (black lines) and that predicted by the TCG and UCG models, employing the global closure assumption for different molecular diffusivity ratios and turbulence indices shown as colored lines.
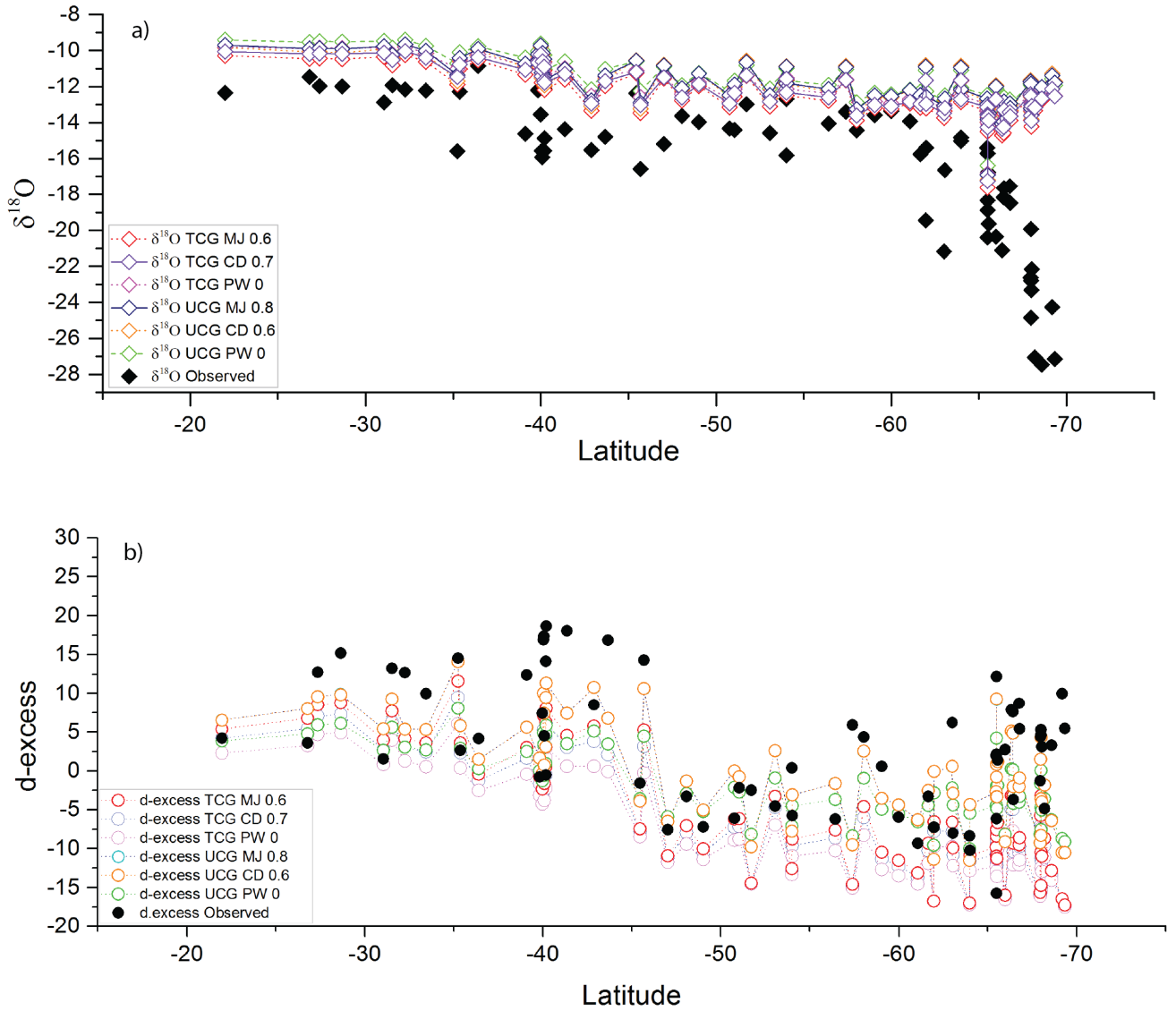
Figure 9. Latitudinal variation of the observed $\delta^{18}O$ (a) as filled black diamonds and d-excess (b) as filled black circles and the modelled values (colored open diamonds and circles) for the model runs where the observed slope is comparable to the modelled slope. The statistical parameters analysis of the observed and modelled regression are listed in Table 3.
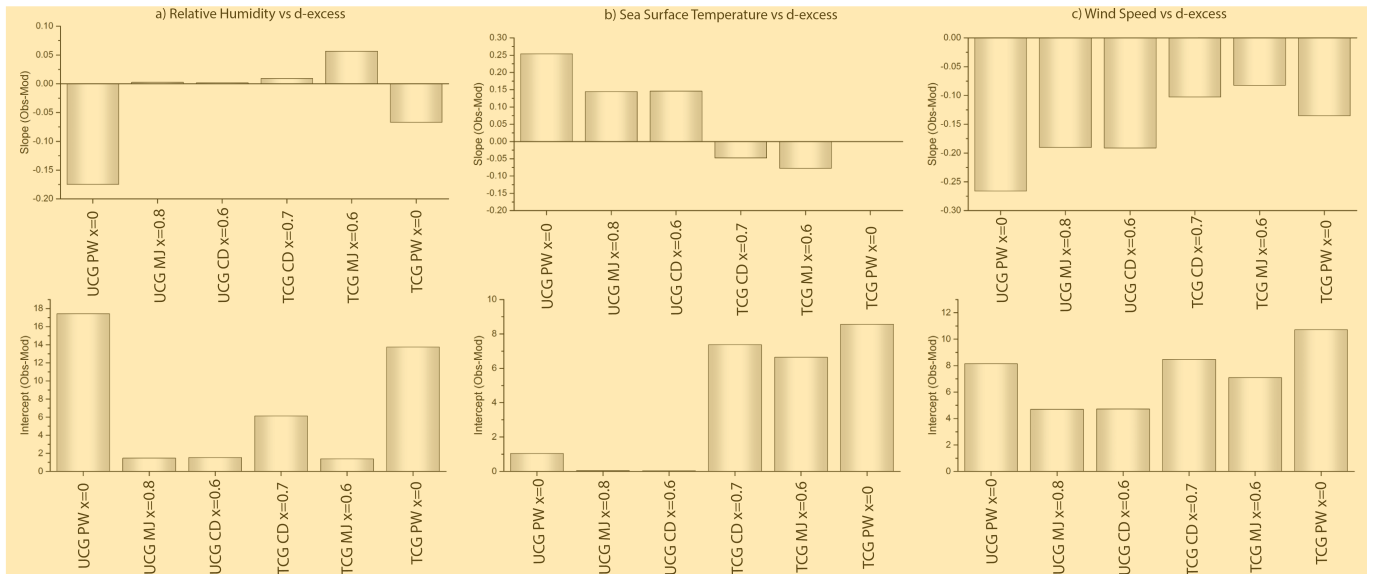
Figure 10. Differences between observed and predicted slopes and intercepts of the relationships between d-excess vs relative humidity, sea surface temperature and wind speed.
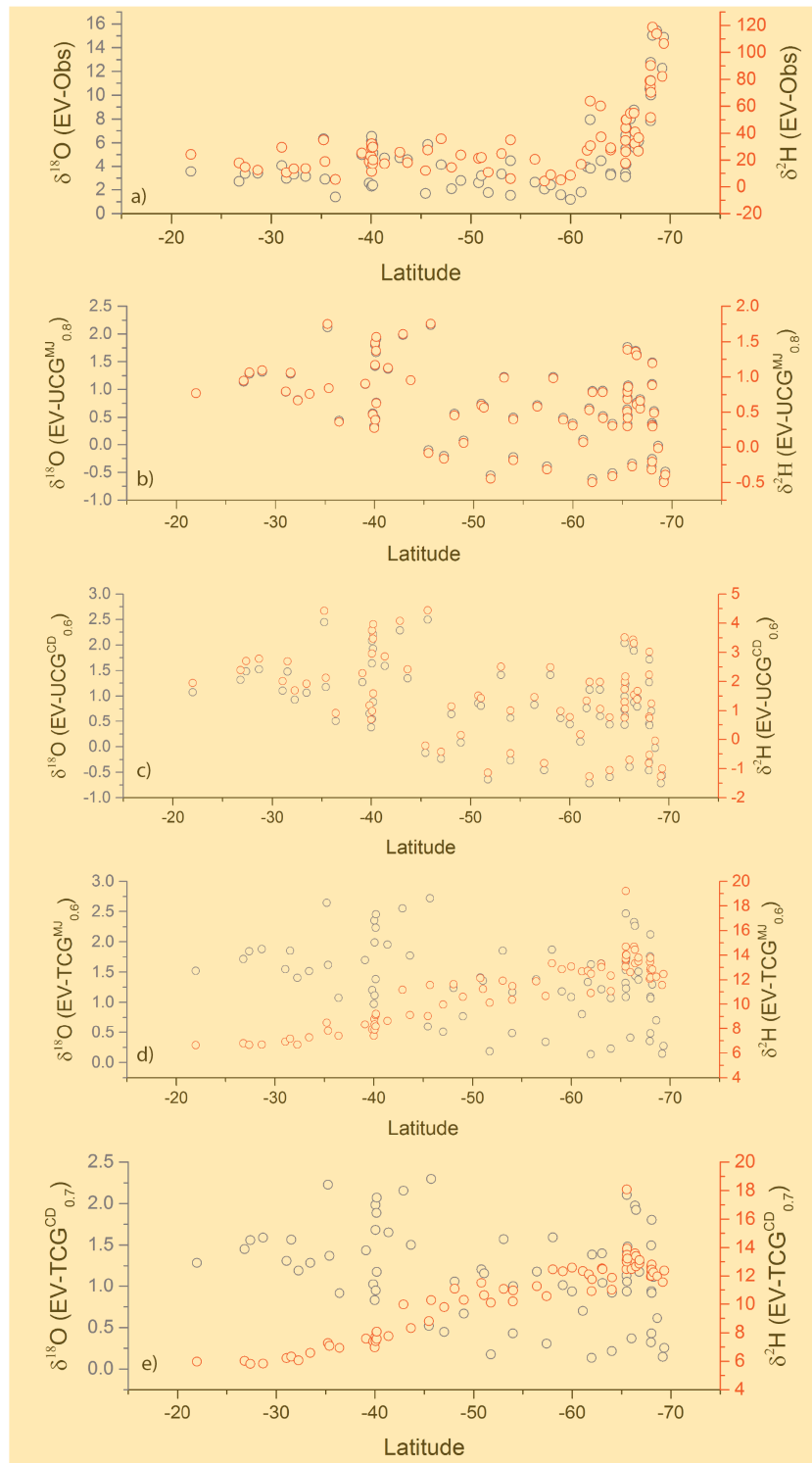
Figure 11. a) the difference between the $\delta^{18}O$ (blue columns) and $\delta^2 H$ (red open circles) of equilibrium vapor and observed water vapor isotopic composition. b-e) shows difference between the $\delta^{18}O$ and $\delta^2 H$ equilibrium vapor and that predicted by the best fit model runs.
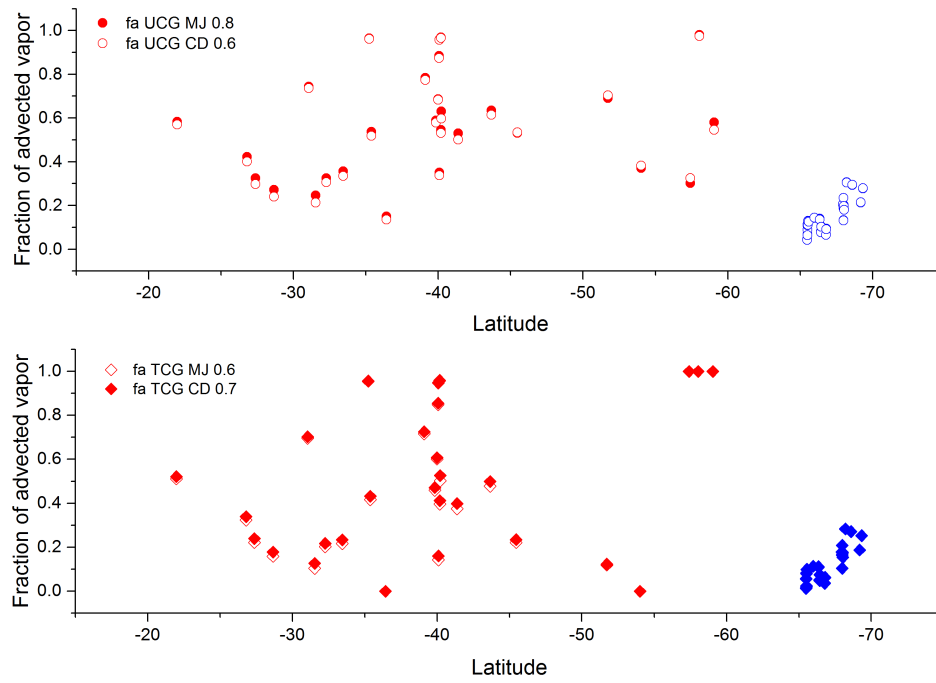
Figure 12. a) Fraction of advected vapor that explains the water vapor isotopic composition for the best fit model runs. Red and blue colors depict the different end member compositions used for calculations.

Table 2. Slope, intercept and r^2 of the linear regression equations between meteorological parameters (relative humidity, sea surface temperature and winds speed) and d-excess for different sample classifications. Also listed are the regression parameters for the data from Uemura et al. (2008).

Met. vs d-excess	Classification	Intercept		Slope		Statistics
		Value	Standard Error	Value	Standard Error	R-Square(COD)
Relative Humidity	ALL	34.31	6.23	-0.40	0.08	0.28
	ALL North of 65°S	46.36	6.57	-0.56	0.08	0.49
	ALL South of 65°S	8.35	12.49	-0.08	0.15	0.01
	SOE IX North of 65°S	57.40	6.15	-0.64	0.08	0.77
	SOE X North of 65°S	48.66	8.28	-0.64	0.11	0.61
	ALL SOE X	53.37	8.93	-0.71	0.12	0.51
	ALL SOE IX	42.72	6.54	-0.45	0.08	0.51
	Uemura All	54.12	4.27	-0.58	0.05	0.66
	Uemura North of 65°S	55.71	5.82	-0.61	0.08	0.62
Sea Surface Temperature	ALL	-1.58	1.15	0.56	0.10	0.31
	ALL North of 65°S	-4.83	1.46	0.74	0.11	0.52
	ALL South of 65°S	0.59	2.06	1.50	1.81	0.03
	SOE IX North of 65°S	-5.54	2.63	0.84	0.16	0.56
	SOE X North of 65°S	-4.18	1.76	0.56	0.16	0.35
	ALL SOE X	-2.19	1.62	0.43	0.18	0.14
	ALL SOE IX	-0.36	1.60	0.58	0.12	0.42
	Uemura All	4.13	0.98	0.79	0.12	0.43
	Uemura North of 65°S	3.43	1.35	0.85	0.13	0.53
Wind Speed	ALL	9.40	1.97	-0.47	0.12	0.18
	ALL North of 65°S	11.68	2.54	-0.53	0.14	0.24
	ALL South of 65°S	7.74	3.22	-0.55	0.25	0.19
	SOE IX North of 65°S	15.16	3.35	-0.61	0.20	0.31
	SOE X North of 65°S	5.93	3.67	-0.33	0.19	0.11
	ALL SOE X	6.08	2.96	-0.38	0.17	0.13
	ALL SOE IX	11.58	2.51	-0.47	0.17	0.20

Table 3. Slope, intercept and r^2 of the linear regression equations between observed and modelled $\delta^{18}O$ and d-excess for the best fit models for samples collected north of 65°S.

Observed vs Modelled		Intercept		Slope		Statistics	
		Value	Standard Error	Value	Standard Error	Adj. R-Square	Root-MSE (SD)
$\delta^{18}O$ All	UCG MJ 0.8	-8.88	0.57	0.18	0.03	0.28	1.15
	UCG CD 0.6	-9.06	0.59	0.17	0.04	0.26	1.20
	TCG MJ 0.6	-9.42	0.57	0.19	0.03	0.30	1.15
	TCG CD 0.7	-9.15	0.55	0.19	0.03	0.32	1.12
$\delta^{18}O$ North of 65°S	UCG MJ 0.8	-6.45	0.89	0.34	0.06	0.38	0.84
	UCG CD 0.6	-6.50	0.91	0.34	0.06	0.38	0.86
	TCG MJ 0.6	-7.02	0.91	0.34	0.06	0.38	0.86
	TCG CD 0.7	-6.89	0.91	0.34	0.06	0.37	0.86
d-excess All	UCG MJ 0.8	-0.94	0.64	0.47	0.07	0.39	5.08
	UCG CD 0.6	-0.94	0.64	0.47	0.07	0.39	5.07
	TCG MJ 0.6	-6.46	0.75	0.58	0.08	0.41	6.00
	TCG CD 0.7	-7.39	0.71	0.55	0.08	0.41	5.66
d-excess North of 65°S	UCG MJ 0.8	-0.35	0.63	0.60	0.07	0.63	4.07
	UCG CD 0.6	-0.36	0.63	0.60	0.07	0.63	4.06
	TCG MJ 0.6	-4.93	0.72	0.74	0.08	0.67	4.67
	TCG CD 0.7	-5.85	0.68	0.70	0.07	0.66	4.41

Supplementary document accompanying the manuscript 'Craig-Gordon model validation using stable isotope ratios in water vapor over the Southern Ocean'

Contents

5

1 Sample collection and isotopic analysis

Atmospheric moisture was sampled using cryogenic cold trap, which is custom-made using pyrex tubes where atmospheric vapor was condensed with the help of a freezing mixture of liquid Nitrogen and Ethanol; maintained the temperature at ≈ -80°C. First, the inlet was connected to the Poly vinyl chloride (PVC) tube which was set at the forecastle of the ship at two different heights as mentioned above. The outlet of the glass trap was connected to a vacuum pump which is maintained at a flow rate of ≈ 250 ml/min. The line was flushed using the pump for at least ≈ 15 Min's before starting the collection process to avoid any sort of residual ambient air inside the tubing and the trap. An Ultra Torr connector (Swagelok) was connected from PVC tubing to the glass flask and from glass trap to the vacuum pump. The sampling time required for generating appreciable amount (2-3ml) of condensed water for isotopic analysis was ≈ 3 to 6 hours depending on the sampling location with greater sampling time at higher latitudes. After the sampling is done both ends of the glass flask was sealed using Parafilm to avoid any air inclusion inside the flask. Atmospheric moisture, condensed inside the cold trap as ice, was allowed to melt at room temperature (≈ 15-20°C) and then transferred into 5 ml polyethylene storage vials. The samples were stored at 4°C. A similar setup for water vapor sampling was presented in the earlier studies Rahul et al. (2016, 2018).

Surface water samples were collected form Conductivity Temperature Depth (CTD) rosette when it was deployed and from a bucket thermometer used for measuring the sea surface temperature. Surface water samples were collected in 50ml High-Density Polyethylene air tight bottles.

All these samples were shipped to Bangalore for isotopic analysis and the measurements were carried out at the Centre for Earth Sciences, Indian Institute of Science, Bangalore. The protocol followed for the analysis of the gases after equilibration using a Finnigan Gas-bench II attached to a MAT 253 mass spectrometer is described in the (Rangarajan and Ghosh, 2011). For oxygen isotope analysis $200\mu L$ of water was transferred into an exetainer vial capped with butyl rubber septa and equilibrated with gas mixture 3% CO2+97% He for a period of 20 hours. For hydrogen isotopes, the water sample was equilibrated with gas mixture of 3% H2+97% He in presence of platinum catalyst (Hokko bead sticks) for a period of 80mins. The isotope ratios are expressed in ‰ using the standard δ notation relative to Vienna Standard Mean Ocean Water (VSMOW). Internal laboratory standards (OASIS-WWW, OASIS-LDK and OASIS-VOULEP) calibrated against the international water standards (VSMOW, Standard Light Antarctic Precipitation, and Greenland Ice Sheet Project) available from International Atomic Energy Agency in Vienna, were used to determine the accuracy and precision of the analysis. To account for intra batch calibration and drift correction, additional internal laboratory standards were measured in a batch. The overall analytical uncertainty on the measurements ($\pm 1\sigma$), as determined from replicate measurements of internal laboratory standards, were respectively ± 1.0‰ and ± 0.1‰ for $\delta^2 H$ and $\delta^{18} O$. Isotopic values are reported here with one standard deviation.

2 Meteorological measurements

Atmosphere readings were taken via multiple instruments on-board the ocean research vessel SA Agulhas. Relative Humidity was calculated from the Psychrometric charts with the help of dry bulb and wet bulb temperature readings from sling Psychrometer with a range of -5°C to +50°C and a least count of 0.2°C. The expected accuracy in the relative humidity measurements from the psychrometer in 2-3%. Air temperature, Atmospheric Pressure, Wind's magnitude and Direction, GPS were logged from AWS (Automatic Weather Station) installed on board the ship. Salinity was measured using an Auto Salino Meter (Tsurumi Seiki Co. Ltd, Japan. Salinity values are expressed in the 1978 Practical Salinity Scale (PSU) (PSS-78) with a precision of ± 0.005 PSU. Sea Surface Temperature (SST) was measured using a bucket thermometer (Theodor Friedrichs and Co, Germany; accuracy $\pm$ 0.5°C).

3 Supplementary figures and tables
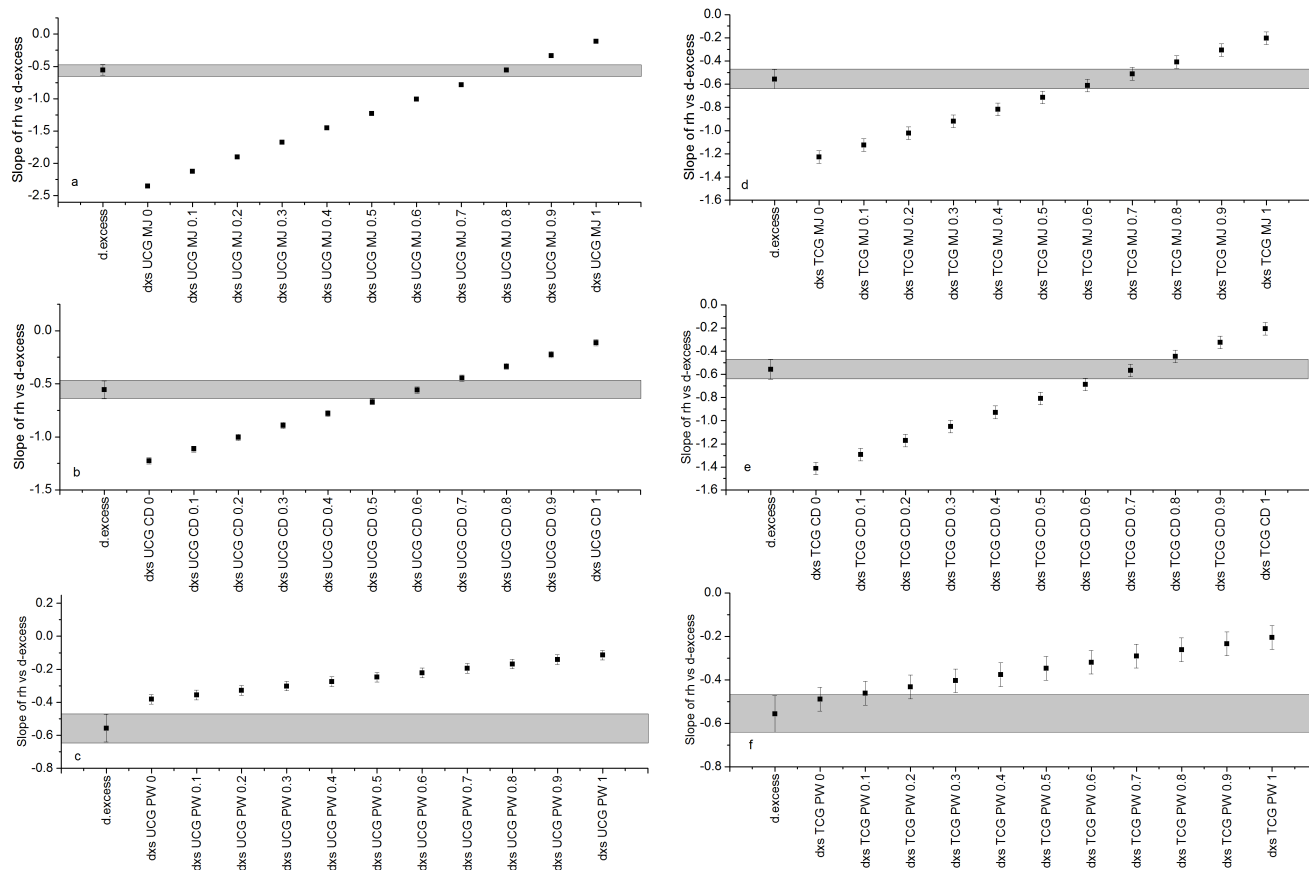
Figure 1. (S) Slope of the relative humidity vs d-excess for the UCG (a-c) and the TCG (d-f) model runs (filled black squares) and the observed value (grey band).
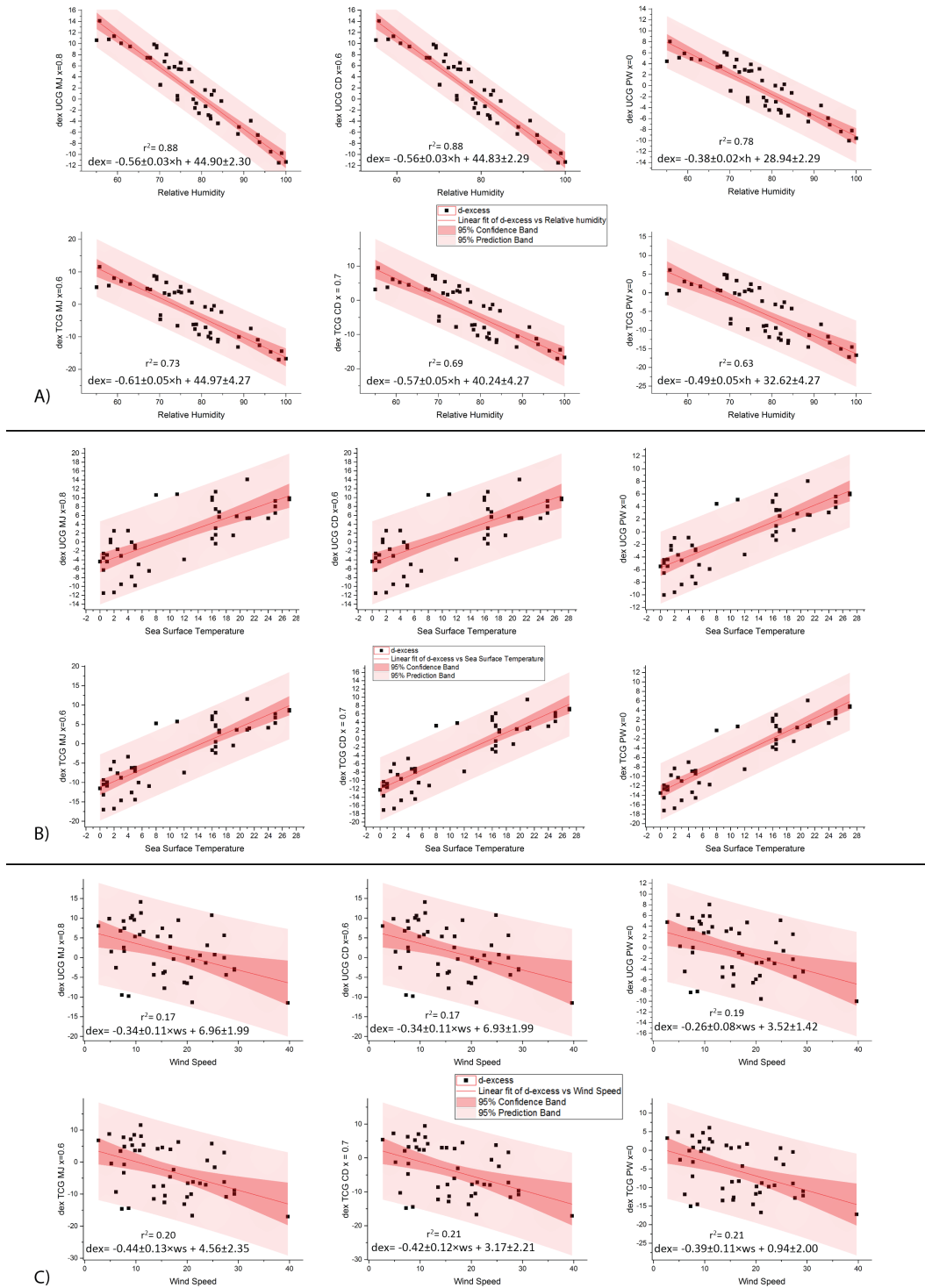
Figure 2. (S) Linear regression equations between relative humidity (A), sea surface temperature (B) and wind speed (C) and the d-excess of the best-fit model runs. The dark and light pink shaded regions depict the 95% confidence bands and 95% prediction bands respectively.

4

Table 1. (S) Slope, intercept and r^2 of the linear regression equations between meteorological parameters (relative humidity, sea surface temperature and winds speed) and $\delta^{18}O$ for different sample classifications. Also listed are the regression parameters for the data from Uemura et al. (2008)

Met. vs $\delta^{18}O$	Classification	Intercept		Slope		Statistics
		Value	Standard Error	Value	Standard Error	R-Square(COD)
Relative Humidity	ALL	-11.43	3.43	-0.06	0.04	0.03
	ALL North of 65°S	-15.49	2.04	0.02	0.03	0.01
	ALL South of 65°S	-11.05	5.11	-0.12	0.06	0.15
	SOE IX North of 65°S	-12.37	2.59	-0.02	0.03	0.01
	SOE X North of 65°S	-18.95	3.39	0.06	0.04	0.07
	Uemura All	-20.61	2.81	0.05	0.04	0.02
Sea Surface Temperature	ALL	-18.43	0.53	0.27	0.05	0.33
	ALL North of 65°S	-15.47	0.40	0.12	0.03	0.27
	ALL South of 65°S	-19.38	0.71	-2.37	0.62	0.41
	SOE IX North of 65°S	-15.30	0.70	0.12	0.04	0.26
	SOE X North of 65°S	-15.52	0.51	0.11	0.05	0.19
	ALL SOE X	-16.82	0.42	0.19	0.05	0.33
	ALL SOE IX	-21.07	0.96	0.41	0.07	0.51
	Uemura All	-17.40	0.46	0.19	0.05	0.16
Wind Speed	ALL	-17.85	1.01	0.10	0.06	0.04
	ALL North of 65°S	-12.74	0.60	-0.09	0.03	0.13
	ALL South of 65°S	-23.76	1.40	0.25	0.11	0.21
	SOE IX North of 65°S	-12.62	0.77	-0.07	0.05	0.11
	SOE X North of 65°S	-13.05	0.98	-0.09	0.05	0.12
	ALL SOE X	-16.66	0.93	0.06	0.05	0.03
	ALL SOE IX	-18.77	1.80	0.14	0.12	0.04

Table 2. (S) Slope, intercept and r^2 of the linear regression equations between meteorological parameters (relative humidity, sea surface temperature and winds speed) and $\delta^2 H$ for different sample classifications. Also listed are the regression parameters for the data from Uemura et al. (2008)

Met. vs $\delta^2 H$	Classification	Intercept		Slope		Statistics
		Value	Standard Error	Value	Standard Error	R-Square(COD)
Relative Humidity	ALL	-57.14	27.50	-0.90	0.35	0.09
	ALL North of 65°S	-77.52	18.79	-0.42	0.24	0.06
	ALL South of 65°S	-41.57	22.20	-0.77	0.27	0.27
	SOE IX North of 65°S	-102.94	28.84	-0.18	0.38	0.01
	SOE X North of 65°S	-133.31	30.61	0.10	0.41	0.00
	Uemura All	-110.71	22.14	-0.16	0.28	0.00
Sea Surface Temperature	ALL	-149.02	3.84	2.76	0.34	0.49
	ALL North of 65°S	-128.58	2.78	1.68	0.20	0.61
	ALL South of 65°S	-127.93	5.09	1.76	0.31	0.60
	SOE IX North of 65°S	-128.31	3.31	1.41	0.30	0.50
	SOE X North of 65°S	-136.73	2.72	1.95	0.30	0.55
	ALL SOE X	-168.91	7.05	3.88	0.53	0.63
	ALL SOE IX	-154.43	5.43	-17.47	4.77	0.39
	Uemura All	-135.09	2.99	2.28	0.36	0.41
Wind Speed	ALL	-133.39	8.50	0.36	0.51	0.01
	ALL North of 65°S	-90.28	5.20	-1.24	0.29	0.29
	ALL South of 65°S	-85.84	6.89	-1.19	0.41	0.29
	SOE IX North of 65°S	-98.47	7.54	-1.04	0.40	0.23
	SOE X North of 65°S	-127.16	7.58	0.07	0.43	0.00
	ALL SOE X	-138.60	15.43	0.63	1.01	0.01
	ALL SOE IX	-182.36	11.09	1.49	0.85	0.13

4 Data used in this study

Table 3. (S) SOE-IX meteorological data, water vapor and surface water isotopic composition.

Date	Lon	Lat	Tair (^0C)	Atm. Pres. ($mbar$)	Rel. Hum. ($\%$)	Wind Speed (m/s)	SST (^0C)	$\delta^{18}O$ ($‰$)	δ^2H ($‰$)	d-excess ($‰$)	Sal. (PSU)	$\delta^{18}O_{SW}$ ($‰$)
08/01/2017	57.50	-27.38	29.60	1015.80	69.31	9.68 =	27.0	-11.97	-83.04	12.71	35.59	
08/01/2018	57.52	-28.66	29.20	1014.80	68.69	4.80	27.0	-12.00	-80.79	15.17	35.50	
09/01/2017	57.49	-31.53	26.13	1016.50	69.31	7.58	25.0	-11.92	-82.11	13.22	35.54	0.31
09/01/2017	57.50	-32.26	24.13	1016.50	77.01	14.25	24.0	-12.16	-84.65	12.66	35.57	
09/01/2017	57.51	-33.44	19.83	1018.67	75.15	9.82	21.0	-12.22	-87.82	9.98	35.41	
10/01/2017	57.50	-35.38	21.50	1019.67	73.54	10.75	19.5	-12.29	-95.66	2.64	35.47	0.33
10/01/2017	57.51	-36.43	21.17	1017.67	82.94	5.20	19.0	-10.86	-82.74	4.16	35.46	
11/01/2017	57.87	-39.11	13.88	1018.25	72.25	27.25	17.0	-14.62	-104.60	12.36	35.58	
12/01/2017	58.41	-40.07	13.67	1027.83	60.86	9.00	16.0	-15.57	-107.66	16.89	35.41	
12/01/2017	57.94	-40.08	12.38	1028.00	67.06	7.75	16.5	-15.91	-109.99	17.33	35.51	
14/01/2017	58.52	-40.09	17.40	1017.80	82.36	25.40	16.0	-11.96	-91.18	4.52	35.36	0.38
13/01/2017	57.99	-40.21	13.00	1025.00	59.18	11.00	16.5	-14.88	-100.35	18.65	35.37	
15/01/2017	59.46	-41.38	14.17	1022.00	67.80	15.17	16.5	-14.37	-96.94	18.03	35.47	0.35
16/01/2017	61.15	-43.67	16.53	1023.83	71.16	7.00	17.0	-14.78	-101.41	16.85	35.49	-0.26*
16/01/2017	62.72	-45.46	11.67	1012.33	91.67	15.33	12.0	-12.37	-100.60	-1.60	35.52	
17/01/2017	64.00	-47.02	7.33	1003.33	93.33	20.00	7.0	-15.19	-129.06	-7.57	33.72	-0.12
18/01/2017	64.10	-49.02	5.60	1008.60	88.86	20.80	5.5	-13.97	-118.99	-7.20	33.52	-0.12
19/01/2017	64.17	-51.05	5.45	1011.67	78.70	21.17	5.0	-14.40	-117.37	-2.18	33.80	-0.07
19/01/2017	67.00	-51.73	4.79	1009.29	98.97	8.57	5.0	-12.97	-106.26	-2.52	33.69	
20/01/2017	68.49	-54.01	4.54	1006.57	93.73	15.57	4.5	-12.68	-101.07	0.37	33.87	0.05*
21/01/2017	69.29	-57.40	4.00	996.25	96.39	7.25	3.0	-13.39	-101.24	5.90	33.89	0.03*
22/01/2017	70.08	-61.95	0.98	970.20	100.00	21.00	2.0	-19.46	-162.93	-7.26	33.61	-0.07
23/01/2017	68.34	-64.00	0.14	976.17	98.31	39.67	0.5	-14.82	-126.91	-8.37	33.83	0.18*
24/01/2017	74.01	-65.99	0.09	983.00	95.57	14.86	0.5	-20.35	-160.07	2.72	33.86	
25/01/2017	72.54	-67.96	-0.51	992.14	96.45	20.57	1.5	-22.62	-182.23	-1.28	33.79	-0.61
26/01/2017	74.01	-67.99	1.00	991.33	72.19	7.67	1.5	-22.79	-177.95	4.41	33.43	
26/01/2017	74.00	-68.00	-0.33	992.00	83.67	12.00	1.5	-19.94	-154.85	4.66	33.21	
31/01/2017	76.00	-68.00	-1.75	978.00	94.23	5.83	1.5	-24.86	-193.54	5.31	32.73	
27/01/2017	74.05	-68.02	1.08	990.00	65.92	5.67	1.5	-23.33	-182.05	4.56	33.38	
30/01/2017	76.12	-68.04	-0.50	988.50	84.14	14.25	1.0	-22.17	-174.22	3.11	32.77	
27/01/2017	73.93	-68.21	0.12	988.40	80.13	8.20	2.0	-27.06	-221.38	-4.87	32.42	
28/01/2017	74.01	-68.60	-2.10	987.00	90.36	5.40	2.0	-27.47	-216.45	3.28		
31/01/2017	75.90	-69.19	-0.92	983.67	100.00	12.67	2.5	-24.25	-184.09	9.94	33.74	
01/02/2017	76.05	-69.34	0.33	991.33	97.92	7.33	0.0	-27.14	-211.65	5.46	32.07	
01/09/2018	74.73	-66.78	0.12	978.42	78.87	25.04	0.0	-17.54	-131.63	8.72	32.73	-0.57
01/02/2018	73.31	-66.80	0.74	989.95	76.64	8.75	0.0	-18.48	-142.40	5.41	33.37	-0.69

* The isotopic composition and salinity values of the surface ocean water are from different bucket samples.

Table 4. (S) SOE-X meteorological data, water vapor and surface water isotopic composition.

Date	Lon	Lat	Tair (^0C)	Atm. Pres. ($mbar$)	Rel. Hum. (%)	Wind Speed (m/s)	SST (^0C)	$\delta^{18}O$ (‰)	δ^2H (‰)	d-excess (‰)	Sal. (PSU)	$\delta^{18}O_{SW}$ (‰)
12/10/2017	57.56	-21.98	26.13	1015.50	75.00	11.50		-12.34	-94.50	4.20		
12/11/2017	57.79	-26.80	28.55	1012.70	71.60	2.70	25.0	-11.46	-88.03	3.61	35.41	0.53
12/12/2017	58.00	-31.05	21.53	1016.00	74.53	16.76	21.5	-12.87	-101.43	1.52	35.42	0.77
13/12/17	58.20	-35.24	19.00	1015.00	55.75	10.93	21.0	-15.58	-110.07	14.54	35.56	0.36
14/12/17	58.49	-39.84	18.00	1007.13	80.82	7.72	16.5	-12.21	-98.43	-0.77	35.51	0.36
15/12/17	57.49	-39.99	14.46	995.03	84.68	17.36	16.5	-13.54	-100.92	7.39	33.84	0.61
16/12/17	58.80	-40.18	14.05	1015.04	63.00	18.29	16.0	-15.56	-110.40	14.11	35.47	0.28
17/12/17	58.38	-40.19	16.93	1016.80	77.68	23.94	16.5	-12.11	-97.43	-0.54	35.46	
18/12/17	60.50	-42.89	9.33	1011.52	57.95	24.82	11.0	-15.52	-115.67	8.51	33.95	
19/12/17	62.63	-45.69	8.07	1015.17	55.04	9.29	8.0	-16.56	-118.22	14.29	34.38	0.08
20/12/17	64.35	-48.07	6.94	991.67	80.92	23.65	5.0	-13.62	-112.24	-3.28	33.90	-0.41
21/12/17	63.85	-50.78	4.52	972.07	78.00	27.25	4.5	-14.31	-120.64	-6.12	33.81	-0.55
22/12/17	65.58	-53.07	4.79	970.60	70.21	7.64	4.0	-14.58	-121.16	-4.54		-0.02
23/12/17	68.23	-54.02	2.26	981.60	82.06	29.24	3.0	-15.81	-132.28	-5.76	33.90	0.02*
24/12/17	69.03	-56.43	2.80	993.74	78.40	13.49	2.5	-14.05	-118.57	-6.19	33.95	-0.01*
25/12/17	70.14	-58.03	3.18	1002.36	70.17	16.68	2.0	-14.44	-111.16	4.33	33.92	-0.57
25-26/12/17	70.12	-59.05	1.80	1002.17	82.14	15.67	0.5	-13.58	-108.05	0.60	33.08	-0.39
26/12/17	71.59	-59.99	1.21	993.15	83.82	13.50	0.0	-13.35	-112.80	-5.97	33.61	-0.48
26/12/17	71.14	-61.06	0.14	984.87	88.64	19.45	0.5	-13.93	-120.74	-9.32	33.68	-0.51
27/12/17	70.90	-61.66	1.19	985.72	79.35	6.12	0.5	-15.74	-129.25	-3.30	33.71	-0.20
17-18/01/18	57.49	-61.99	2.80	986.17	74.25	20.14	1.5	-15.39	-130.38	-7.28	33.70	
28/12/17	69.99	-63.01	-1.02	990.34	74.22	22.52	1.5	-21.18	-163.28	6.18	33.63	-0.59
17/01/18	57.52	-63.05	1.16	974.27	81.60	29.23	1.0	-16.63	-141.06	-8.01	33.49	
16-17/01/18	57.42	-64.01	1.90	969.20	83.90	27.63	1.0	-15.02	-130.43	-10.24	33.20	-0.22*
14/01/18	66.99	-65.49	-0.70	971.30	79.66	17.03	0.0	-15.40	-121.20	2.00		-0.35
16/01/18	57.85	-65.51	1.34	967.24	84.00	27.02	1.0	-15.70	-141.37	-15.73	33.57	-1.05*
30/12/17	74.91	-65.51	-0.36	978.48	76.16	6.21	0.0	-18.88	-148.91	2.15	33.39	-0.62
10/01/2018	68.81	-65.51	0.31	980.96	61.30	4.00	-0.5	-20.40	-151.04	12.15	33.69	-3.45*
31/12/17	73.84	-65.52	-0.40	984.47	74.00	14.10	0.0	-18.33	-152.82	-6.18	33.51	-1.16*
31/12/17-1/1/18	72.67	-65.54	-0.25	988.00	81.50	16.40	-1.0	-16.77	-157.86	-23.71	33.61	-0.80
15/01/18	57.26	-65.58	-0.33	973.95	72.66	11.08	0.5	-19.64	-155.75	1.40	33.48	
29-30/12/17	74.79	-66.35	-1.35	982.00	62.50	7.00	-0.5	-21.11	-161.02	7.88	32.99	-0.64
07/01/2018	74.98	-66.43	1.86	981.77	63.53	4.88	0.0	-18.17	-137.79	7.59	32.73	
01/01/2018	73.00	-66.45	0.90	987.10	77.67	5.60	-0.5	-17.65	-144.89	-3.72	32.73	-0.33*
09/01/2018	74.73	-66.78	0.12	978.42	78.87	25.04	0.0	-17.54	-131.63	8.72	32.73	-0.57
02/01/2018	73.31	-66.80	0.74	989.95	76.64	8.75	0.0	-18.48	-142.40	5.41	33.37	-0.69

50   * The isotopic composition and salinity values of the surface ocean water are from different bucket samples.

8

References

Rahul, P., Ghosh, P., Bhattacharya, S., and Yoshimura, K.: Controlling factors of rainwater and water vapor isotopes at Bangalore, India: Constraints from observations in 2013 Indian monsoon, Journal of Geophysical Research: Atmospheres, 121, 2016.

55 Rahul, P., Prasanna, K., Ghosh, P., Anilkumar, N., and Yoshimura, K.: Stable isotopes in water vapor and rainwater over Indian sector of Southern Ocean and estimation of fraction of recycled moisture, Scientific reports, 8, 2018.

Rangarajan, R. and Ghosh, P.: Role of water contamination within the GC column of a GasBench II peripheral on the reproducibility of 18O/16O ratios in water samples, Isotopes in environmental and health studies, 47, 498–511, 2011.

Uemura, R., Matsui, Y., Yoshimura, K., Motoyama, H., and Yoshida, N.: Evidence of deuterium excess in water vapor as an indicator of
60 ocean surface conditions, Journal of Geophysical Research: Atmospheres, 113, 2008.